University of Alberta

Effects of Channel Estimation Errors on Receiver Selection Combining Diversity for Alamouti MIMO Systems

by

Wenyu Li

A thesis submitted to the Faculty of Graduate Studies and Research in partial fulfillment of the requirements for the degree of **Master of Science**.

Department of Electrical and Computer Engineering

Edmonton, Alberta

Spring 2005

Library and Archives Canada

Published Heritage Branch

395 Wellington Street
Ottawa ON K1A 0N4
Canada

Bibliothèque et Archives Canada

Direction du Patrimoine de l'édition

395, rue Wellington
Ottawa ON K1A 0N4
Canada

Your file Votre référence
ISBN: 978-0-494-22424-3
Our file Notre référence
ISBN: 978-0-494-22424-3

NOTICE:
The author has granted a non-exclusive license allowing Library and Archives Canada to reproduce, publish, archive, preserve, conserve, communicate to the public by telecommunication or on the Internet, loan, distribute and sell theses worldwide, for commercial or non-commercial purposes, in microform, paper, electronic and/or any other formats.

The author retains copyright ownership and moral rights in this thesis. Neither the thesis nor substantial extracts from it may be printed or otherwise reproduced without the author's permission.

AVIS:
L'auteur a accordé une licence non exclusive permettant à la Bibliothèque et Archives Canada de reproduire, publier, archiver, sauvegarder, conserver, transmettre au public par télécommunication ou par l'Internet, prêter, distribuer et vendre des thèses partout dans le monde, à des fins commerciales ou autres, sur support microforme, papier, électronique et/ou autres formats.

L'auteur conserve la propriété du droit d'auteur et des droits moraux qui protège cette thèse. Ni la thèse ni des extraits substantiels de celle-ci ne doivent être imprimés ou autrement reproduits sans son autorisation.

In compliance with the Canadian Privacy Act some supporting forms may have been removed from this thesis.

While these forms may be included in the document page count, their removal does not represent any loss of content from the thesis.

Conformément à la loi canadienne sur la protection de la vie privée, quelques formulaires secondaires ont été enlevés de cette thèse.

Bien que ces formulaires aient inclus dans la pagination, il n'y aura aucun contenu manquant.

Canada

Abstract

Multiple-input and multiple-output (MIMO) systems improve wireless system performance by exploiting the multiple transmission paths between transmitters and receivers. However, hardware implementations based on multiple antennas are generally expensive. This, therefore, stimulates the need for low-cost, low-complexity techniques that possess the benefits of multiple antennas. Antenna selection (where the "best" antennas are selected) is one such technique. This thesis analyzes the bit error rate (BER) performance of several selection schemes for a simple MIMO system - the Alamouti MIMO system. The system performance of binary phase-shift keying (BPSK) modulation is investigated. In addition to the pre-existing selection schemes, two new selection schemes, which do not require knowledge of channel gain for selection, are proposed. Simulation results show the proposed schemes to offer comparable performance to that of existing schemes but with simpler hardware requirements. As all selection schemes require the estimation of the transmission channel gain when implementing the coherent detection, the effects of channel estimation error on these selection systems are analyzed and quantified.

Acknowledgements

I would like to express my sincere gratitude to all the people who helped me complete this thesis.

First, I want to thank my supervisor Dr. Norman C. Beaulieu for his research guidance, academic discussions, and financial support. I would also like to thank all my colleagues in the *i*CORE Wireless Communications Laboratory for creating an excellent working and studying environment. Particularly, I am greatly indebted to Pavel Loskot for offering academic inspiration and valuable technical discussions.

I wish to express my deep appreciation to Marco Dragic for his encouragement, support, and generous help throughout my research. I warmly thank Ang Li and Bin Li for their friendship and help, especially during the challenging periods.

I also wish to thank David Clyburn for revising my manuscript, and offer my special gratitude to Paul Piva for his assistance in proofreading my thesis.

Finally, I owe my most sincere gratitude to my parents and my brother. Without their understanding and loving support, it would have been impossible for me to complete this work.

This thesis was financially supported through the Natural Sciences and Engineering Research Council of Canada (NSERC) and the Alberta Informatics Circle of Research Excellence (iCORE).

To my parents

Contents

1 Introduction 1

1.1 Background and Motivation 1

1.2 Literature Review 3

1.3 Thesis Outline and Contributions 5

2 Diversity and Combining Schemes 7

2.1 Fading Channel Models 7

2.1.1 Mathematical Model 8

2.1.2 Small-Scale Fading 9

2.1.3 Rayleigh Fading 10

2.2 Diversity Schemes 10

2.2.1 Microscopic Diversity and Macroscopic Diversity 10

2.2.2 Receiver Diversity and Transmitter Diversity 11

2.2.3 Diversity Classifications 12

2.3 Combining Techniques 14

2.3.1 Selection Combining 14

2.3.2 Switch-and-Stay Combining 14

2.3.3 Maximal Ratio Combining 14

2.3.4 Equal Gain Combining 15

2.3.5 Generalized Selection Combining 15

2.4 Selection Combining Schemes 15

2.4.1 SNR Selection 16
2.4.2 $S+N$ Selection 16
2.4.3 $|ar|$ Selection 17
2.4.4 $|a\omega|$ Selection 18
2.5 Comparisons of Selection Combining Schemes 19

3 Space-Time System and Channel Estimation Error **21**
3.1 Space-Time Wireless Communication Systems 22
3.1.1 Introduction 22
3.1.2 Antenna Configurations 22
3.1.3 Space-Time System Structure 23
3.1.4 Space-Time Coding 24
3.2 Alamouti Scheme 25
3.2.1 The Encoding and Transmission Sequence 25
3.2.2 The Combining Scheme 27
3.2.3 The Decision Rule 27
3.3 Fading Estimation Error 28
3.4 Channel Estimation Error for Pilot Symbol Assisted Modulation in an Alamouti System 29
3.4.1 Fading Estimation in PSAM 29
3.4.2 Derivation of R_c 31
3.4.3 Derivation of $\sigma_{\hat{g}}^2$ 31
3.4.4 Derivation of ρ 32
3.5 Conclusion 32

4 Effects of Channel Estimation Errors on Receiver Selection Combining Schemes for Alamouti MIMO Systems **33**
4.1 Introduction 33
4.2 Bit Error Rate Analysis 35
4.2.1 LLR selection combining 36

4.2.2 *SNR* Selection Combining 39
4.2.3 Switch-and-Stay Selection 42
4.2.4 MRC Diversity 45
4.3 Numerical Results and Discussion 47
4.4 Conclusion 48

5 Receiver Selection Diversity Schemes without Channel Estimation for Alamouti MIMO Systems **57**
5.1 Introduction 57
5.2 New Selection Combining Methods 59
5.2.1 Method 1: Space-Time Square-Law Selection 59
5.2.2 Method 2: Space-Time Magnitude Selection 61
5.3 Numerical results and discussion 63
5.4 Conclusion 65

6 Conclusions **74**

References **77**

List of Figures

2.1 The BER versus SNR for four selection combining schemes and MRC. . . 20

3.1 A space-time wireless communication system. 23

3.2 The Alamouti system with two transmitter antennas and one receiver antenna (after [1, Fig. 2]). 26

4.1 The LLR receiver selection system model. 37

4.2 The envelope-LLR receiver selection system model. 40

4.3 The SNR receiver selection system model. 41

4.4 The SSC receiver selection system model. 43

4.5 The MRC receiver system model. 46

4.6 The BER versus SNR for the 2 TX and 2 Rx, space-time block code with $\rho = 1$. 49

4.7 The BER versus SNR for the 2 TX and 2 Rx, space-time block code with $\rho = 0.9$. 50

4.8 The BER versus SNR for the 2 TX and 2 Rx, space-time block code with $\rho = 0.75$. 51

4.9 The BER versus SNR for the 2 TX and 4 Rx, space-time block code with $\rho = 1$. 52

4.10 The BER versus SNR for the 2 TX and 4 Rx, space-time block code with $\rho = 0.9$. 53

4.11 The BER versus SNR for the 2 TX and 4 Rx, space-time block code with $\rho = 0.75$. 54

4.12 The PSAM BER versus SNR for the 2 Tx and 2 Rx, Alamouti space-time block code with Hamming windowing applied to a sinc interpolator for $K = 30, N = 14$ and $f_D T_s = 0.03$ with symbol location at $n = 3$. 55
4.13 The PSAM BER versus SNR for the 2 Tx and 4 Rx, Alamouti space-time block code with Hamming windowing applied to a sinc interpolator for $K = 30, N = 14$ and $f_D T_s = 0.03$ with symbol location at $n = 3$. 56

5.1 The STSL receiver selection system model. 60
5.2 The STM receiver selection system model. 62
5.3 The BER versus SNR for the 2 TX and 2 Rx, space-time block code with perfect channel estimation. 66
5.4 The BER versus SNR for the 2 TX and 2 Rx, space-time block code with ρ=0.9. 67
5.5 The BER versus SNR for the 2 TX and 2 Rx, space-time block code with ρ=0.75. 68
5.6 The BER versus SNR for the 2 TX and 4 Rx, space-time block code with perfect channel estimation. 69
5.7 The BER versus SNR for the 2 TX and 4 Rx, space-time block code with ρ=0.9. 70
5.8 The BER versus SNR for the 2 TX and 4 Rx, space-time block code with ρ=0.75. 71
5.9 The PSAM BER versus SNR for the 2 TX and 2 Rx, space-time block code with Hamming windowing applied to a sinc interpolator for $K = 30$, $N = 14$ and $f_D T_s = 0.03$ with symbol location at $n = 3$. 72
5.10 The PSAM BER versus SNR for the 2 TX and 4 Rx, space-time block code with Hamming windowing applied to a sinc interpolator for $K = 30$, $N = 14$ and $f_D T_s = 0.03$ with symbol location at $n = 3$. 73

Acronyms

Acronyms	Definition
AWGN	additive white Gaussian noise
BER	bit error rate
BPSK	binary phase shift keying
CDF	cumulative distribution function
CDMA	code division multiple access
EGC	equal gain combining
GSC	generalized selection combining
ISI	inter symbol interference
LLR	log-likelihood ratio
MIMO	multiple-input and multiple-output
MIMO-MU	multiple-input and multiple-output multiuser
MISO	multiple-input and single-output
ML	maximum-likelihood
MRC	maximum ratio combining
PCS	personal communication systems
PDF	probability density function
PSAM	pilot symbol assisted modulation
Rx	receiver
RF	radio frequency
SC	selection combining

SIMO	single-input and multiple-output
SISO	single-input and single-output
SNR	signal-to-noise ratio
SSC	switch-and-stay combining
ST	space-time
STBC	space-time block code
STTC	space-time trellis code
STM	space-time magnitude
STSL	space-time square-law
Tx	transmitter
UHF	ultra high frequency
W-CDMA	wideband CDMA

List of Symbols

Symbol	Definition
a_i	fading amplitude in the *i*th receiver branch
b	normalized R_c
$d_{j,i}$	as defined in (3.5)
E_b	energy per bit
f_D	Doppler spread
$f_A(\alpha_i)$	pdf of α_i
$f_{A_{max}}(\alpha)$	pdf of $\max(\alpha_i)$
$f(x)$	pdf of x
$f_{r_i}(x)$	pdf of r_i
$f_R(r_1)$	pdf of r_1
$F_X(x)$	cdf of x
g_I	in-phase component of the complex fading channel gain
g_{Ik}^n	real part of g_k^n
g_i	complex fading gain in the *i*th receiver branch
$g_{j,i}$	complex fading gain between the *j*th transmitter antenna and the *i*th receiver antenna
$g_{j,i,k}^n$	fading gain between the *j*th transmitter antenna and the *i*th receiver antenna at the *n*th symbol cluster of the *k*th data frame
g_k^n	the complex fading gain at the *n*th symbol cluster of the *k*th data frame
g_Q	quadrature component of the complex fading channel gain

$\hat{g}_{Ik}^n$	real part of $\hat{g}_k^n$
$\hat{g}_j$	estimate of g_j
$\hat{g}_{j,i}$	estimate of $g_{j,i}$
$\hat{g}_{j,i,k}^n$	estimate of $g_{j,i,k}^n$
$\hat{g}_k^n$	estimate of g_k^n
$h_c(t)$	impulse response of the channel
h_k^n	interpolation coefficient for the nth symbol cluster in the kth data frame
$J_0(\cdot)$	zeroth order Bessel function of the first kind
k	data frame index
K	interpolator size
L	number of antennas
L_r	number of receiver antennas
L_s	number of selected antennas
L_t	number of transmitter antennas
$m(t)$	small scale fading component
n	symbol cluster index
n_i	additive noise in the ith receiver branch
n_i^c	combined noise sample in the ith receiver branch
$n_{j,i}$	additive noise at jth symbol interval in the ith receiver branch
$n_{j,k}^n$	the additive noise at the jst symbol interval of the nth symbol cluster of the kth data frame
$n_{j,i,k}^n$	the additive noise at the jnd symbol interval in the nth symbol cluster of the kth data frame in the ith receiver branch
$n(t)$	additive noise source
N	data frame size
N_0	noise power spectral density
P_b	bit error rate
$p(r)$	pdf of r
$Q(\cdot)$	Q-function, the area under the tail of the Gaussian PDF

$Q^{-1}(\cdot)$	inverse Q-function
r	envelope amplitude of the received signal
$r_{j,i}$	sampled received signal at the jth symbol interval in the ith receiver branch
$r(t)$	received signal in continuous time domain
$r_0(t)$	large scale fading component
r_1	as defined in (4.8)
$r_i, i! = 1$	real part of $y'_{j,i}$
$r^n_{j,i,k}$	received signal at the jst symbol interval in the nth symbol cluster of the kth data frame in the ith receiver branch
$Re(x)$	real part of x
R_c	cross-correlation of g_I and $\hat{g}_I$ or g_Q and $\hat{g}_Q$
R_{cs}	cross-correlation of g_I and $\hat{g}_Q$ or $\hat{g}_I$ and g_Q
$R(\tau)$	autocorrelation of the real part of the fading gain
$sgn(x)$	sign of x
$s(t)$	transmitted signal in continuous time domain
$s_j, j = 1,2$	sampled transmitted BPSK signalling
$s^n_{j,i,k}$	the transmitted symbol at the jnd symbol interval in the nth symbol cluster of the kth data frame in the ith receiver branch
$\hat{s}_j$	estimate of s_j
$\hat{s}^n_{j,i,k}$	estimate of $s^n_{j,i,k}$
T_s	symbol interval
x	BPSK signalling
y	normalized MRC output
y_j	space-time combiner output at jth symbol interval
$y_{j,i}$	space-time combiner output at jth symbol interval in ith receiver branch
$y'_{j,i}$	normalized $y_{j,i}$
α_i	normalized combined fading power in the ith receiver branch
$\bar{\gamma}_b$	average SNR per bit
$\bar{\gamma}_c$	effective SNR

γ_c	instantaneous effective SNR
$\gamma_{c,i}$	instantaneous effective SNR at the *i*th receiver branch
γ_{th}	effective SNR threshold
γ_{th}^*	optimal effective SNR threshold
$(\Delta_f)_c$	channel coherent time
$(\Delta_t)_c$	channel coherent bandwidth
η_i	additive Gaussian noise in the *i*th branch after phase compensation
Λ_i	log-likelihood ratio in the *i*th receiver branch
ρ	squared amplitude of the cross-correlation coefficient of the channel fading and its estimation
σ^2	as defined in (2.5)
σ_g^2	variance of the real (imaginary) component of fading gain
$\sigma_{\hat{g}}^2$	variance of the real (imaginary) component of fading gain estimate
σ_n^2	variance of the real (imaginary) component of complex additive noise
σ_r^2	variance of envelope amplitude of the received signal
τ	delay spread
ϕ_i	fading phase in the *i*th branch
ω_i	sampled lowpass received signal before phase compensation in the *i*th receiver branch with single transmitter

Chapter 1

Introduction

1.1 Background and Motivation

In a world of increasing mobility, wireless communications satisfies people's desire to communicate with each other and have access to information regardless of the location of the individuals or the information. Whenever we make a phone call to anyone on this planet using mobile phone, or browse internet in an airport wireless hot spot, we expect an efficient, reliable communication service. This demand has led to the need for techniques that can improve the quality of service in wireless communication systems.

Communication systems support the transmission of information from a source to one or more destinations. Of particular importance in the analysis and design of these communication systems are the characteristics of the physical medium through which the information is transmitted [2]. In wireless transmission, the physical medium may be the atmosphere (free space). Its essential feature is that it corrupts the transmitted signal in a random manner by a variety of possible mechanisms, such as multiplicative signal fading due to the time-variant multipath characteristics of the channel. These features cause the distortion of the transmitted signals before they arrive at the destinations.

The distortion of the transmitted signal limits a higher data rate and a better quality of service, which are desirable in modern wireless communication systems. Many tech-

niques have been used to overcome this disadvantage. A multiple-input and multiple-output (MIMO) system is one of them. In a MIMO system, L_t transmitter antennas are used to transmit information signals and L_r receiver antennas are used to receive these transmitted signals. Compared to traditional single-input and single-output (SISO) systems, MIMO systems employ more transmission paths between transmitters and receivers. As was mentioned in the previous paragraph, wireless media have a random nature which means sometimes better sometimes worse characteristics. If the radio channels consisting of multiple paths in a MIMO system are sufficiently separated in space, time, frequency, or polarization, it is unlikely that they will experience bad distortion together. By carefully combining the signals from multiple paths together or simply selecting the "best" signals among all the received signals, the chance of getting a less distorted received signal is greatly increased compared to that in a SISO system. Thus, MIMO communication techniques have become an important area of focus for next-generation wireless systems [3].

However, MIMO systems with L_t transmitter and L_r receiver antennas require $L_t + L_r$ complete radio frequency (RF) chains at both the transmitter and the receiver, including low-noise amplifiers, down-converters, and analog-to-digital converters. While additional digital signal processing elements may come very cheap, the analog RF elements are still expensive. This brings the drawback of any MIMO system, i.e. the increased complexity and cost. Due to this reason, there is now increasing interest in antenna selection schemes, where the "best" L_s out of L antennas (either at one, or at both link ends) are chosen, down-converted, and processed. This reduces the number of required RF chains, and thus leads to significant savings. The savings come at a price of a usually small performance loss compared to the full-complexity system. Therefore, how to select the antennas in an efficient manner to obtain fairly good performance but still with low cost becomes a very interesting and popular topic. This is also the motivation of the work in this thesis.

In MIMO selection, the "best" branches are chosen under the assumption that they experience the "least" distortion paths. This assumption is based on the channel estimation of these paths at the receivers. This estimation, e.g., which can be generated from pilot signals transmitted along with data signals, is impossibly 100% accurate due to the imperfection

of the estimation method and the uncertainty of the wireless transmission medium. Therefore, the accuracy of the channel estimation plays an important role in antenna selection. As a still relatively unexplored problem [4], the effect of channel estimation errors on the performance of MIMO selection is also investigated in this thesis.

Thus, this work consists of the research of effects of channel estimation errors on selection schemes for MIMO systems. Particularly, we investigate one specific type of MIMO system – the Alamouti MIMO system. This system utilizes only two transmitter antennas and multiple receiver antennas. Owing to the size and power limitation, most of the current hand-held devices can only accommodate at most two antennas, so the Alamouti scheme becomes particularly useful and has been proposed for both the wideband code division multiple access (W-CDMA) and CDMA-2000 standards. Uncoded binary phase-shift keying (BPSK) modulation is used throughout this work. As the simplest modulation technique, BPSK makes the system analysis simpler but the results obtained in this work still provide useful guidance to other higher level modulations. The criteria used to evaluate the overall system performance is bit error rate (BER).

1.2 Literature Review

MIMO antenna selection combining includes receiver (Rx) antenna selection, transmitter (Tx) antenna selection and joint Tx/Rx selection. Since MIMO systems can improve wireless communication in two different ways, i.e., diversity methods and spatial methods [4], selection algorithms and performance analysis for MIMO selection schemes are also developed into two corresponding ways. One focuses on exploiting the multiple paths between Tx and Rx antennas and investigating methods to improve the error rate performance. The other takes advantage of spatial multiplexing, and studies the impact of MIMO systems on the channel capacity.

MIMO Rx selection assumes L_s out of L_r Rx antennas are selected while the Tx uses all available antennas. In [5]- [7], different algorithms are proposed to maximize the channel capacity. Due to the complexity of describing the statistics of all the L_s selected branches,

an upper bound on the capacity is derived in [5]. A lower bound on the outage capacity is presented in [6]. In [8]- [10], the Rx selection criterion is chosen in the sense of achieving the maximum received signal-to-noise ratio (SNR). An approximation of pairwise error probability is given in [8]. An upper bound on pairwise error probability is presented in [9]. In [10], an upper bound on BER is derived.

Tx selection is possible when the channel information is fed back from the receivers. In [11] and [12], Tx antenna selection algorithms are discussed based on channel capacity for low-rank channels. In [13], Tx antenna selection is considered for a zero-forcing spatial multiplexing system. The selection rules are developed for two cases, maximizing ergodic capacity and minimizing the average probability of error. Many other papers chose the optimal selection rules based on optimizing the total received signal power or SNR gain at the receiver [14]- [17]. In these works, the performance analysis of channel capacity, outage probability and symbol error rate or BER are discussed. In [15], the BER analysis of nonideal Tx antenna selection with slow Tx update rate is also included.

Recently, there has been increasing interest in employing antenna selection at both the Tx and Rx side. In [18]- [20], the authors proposed several selection algorithms to select a subset of MIMO Tx and Rx antennas in response to different channel conditions to minimize the average probability of error. In [20], two selection rules are proposed to maximize the channel Frobenius norm when exact channel knowledge is available or to maximize the determinant of the covariance of the vector channel when only statistical channel knowledge is known. In [14], the optimal selection rule is presented to improve the average SNR gain. In [19], by assuming that only knowledge of the second order statistics of the channel is known, the selection criterion with both the maximum likelihood and zero-forcing receivers is derived, motivated by minimizing the average symbol error rate. In [21], a subset of antennas is selected to maximize the average mutual information.

However, most previous work considers the channel state is perfectly known by transmitters or receivers, which unlikely happens in practice. Only a few works take imperfect channel state information into account. In [15], nonideal channel information is assumed as the update rate of channel information at the transmitter side is small compared to the

Doppler fading rate for transmitter selection. The probability density function (pdf) of the received SNR is given, but the average BER cannot be solved in closed-form. Instead, the BER integral is evaluated numerically. In [16], a noisy channel estimation from pilot symbols is considered for transmitter selection. The impact of the SNR of pilot symbols on channel capacity is simulated and measured. However, no analytical expression is given.

1.3 Thesis Outline and Contributions

This thesis consists of six chapters. The first chapter gives the basic background and motivations to the research topic. Impressive improvement in capacity and bit error rate have motivated the recent interest in MIMO systems. However, the multiple RF chains associated with multiple antennas are costly in terms of size, power, and hardware. Antenna selection is a low-cost low-complexity alternative to capture many of the advantages of MIMO systems. Thus, selection schemes for MIMO systems is the main focus of this thesis.

Chapter 2 gives a more detailed technical background for the whole thesis. It describes the characteristics of a wireless propagation environment and the techniques used to overcome the received signal deterioration problem associated with it. As commonly used approaches to combat the wireless propagation environment, several diversity schemes and combining techniques are introduced. Among various diversity combining techniques, selection combining is the simplest. Thus, at the end of this chapter, a summary of several different selection combining methods is provided. A performance comparison of these selection schemes is also given.

Chapter 3 gives the system model used in this work. It comprises four sections. The first section introduces space-time systems. The system structure and coding techniques specific to this system are given. As the simplest type of space-time system, the Alamouti system is illustrated in the second section. Three functions of this scheme: the encoding and transmission sequence of information symbols at the transmitter, the combining scheme at the receiver, and the decision rule for maximum-likelihood detection, are ex-

plained in detail. Section 3 gives an introduction to channel estimation error because, in Alamouti diversity systems, channel estimation is needed for both space-time combiners and selection schemes. The last section gives a detailed examination of channel estimation error for an Alamouti system using one effective channel estimation technique, pilot symbol assisted modulation (PSAM).

In Chapter 4, the system performance of several existing selection methods in Alamouti MIMO systems is analyzed. The BER of BPSK in Rayleigh fading using the Alamouti transmission scheme and receiver selection diversity in the presence of channel estimation error is studied. Closed-form expressions for the BER of log-likelihood ratio selection, signal-to-noise ratio selection, switch-and-stay combining selection and maximum ratio combining are derived in terms of the SNR and the cross-correlation coefficient of the channel gain and its corrupted estimate. The effects of channel estimation errors on each selection scheme are examined.

In Chapter 5, two new receiver selection schemes, space-time square-law selection diversity and space-time magnitude selection diversity, are proposed for a MIMO system using the Alamouti scheme at the transmitter in a slow, flat Rayleigh fading channel. They are proved to provide almost the same performance as SNR selection, but with much simpler implementations. The BER of BPSK in Rayleigh fading using these two selection schemes is studied and compared to that of previous selection schemes. The effects of channel estimation errors on each selection scheme are examined.

Chapter 6 is the conclusion of the thesis' contributions.

Chapter 2

Diversity and Combining Schemes

In this chapter, we describe the characteristics of a wireless propagation environment and the techniques used to overcome the received signal deterioration problem associated with it. Section 2.1 presents a mathematical model for the so-called fading channel, and categories of fading channels are examined. A particular fading model, the Rayleigh fading channel, which is analyzed in this thesis, is described. Commonly used approaches to combat fading, i.e. diversity schemes and combining techniques, are introduced in Section 2.2 and Section 2.3, respectively. Among various diversity combining techniques, selection combining is the simplest. Section 2.4 summarizes several different selection combining methods. A performance comparison of these selection schemes is given in Section 2.5.

2.1 Fading Channel Models

The simplest mathematical model for an imperfect communication channel is the additive noise channel. In this model, the transmitted signal is corrupted only by additive noise. When the additive noise physically comes from the thermal noise generated in electronic components and amplifiers in a receiver, it can be statistically characterized as a Gaussian noise process. Thus, the corresponding communication channel is called the additive white Gaussian noise (AWGN) channel [2]. This is a simple model because it assumes that the transmission media are ideal.

However, in a wireless communication system, signal propagation takes place in the atmosphere or near the ground. Unlike wired channels that are stationary and predictable, there are always some objects between the transmitter and receiver antennas that might absorb, reflect, diffract, and scatter a propagating electromagnetic wave. As a result, the propagating signal can travel from the transmitter to the receiver over multiple reflective paths, and these different propagation paths cause the signal to arrive at the receiver with different time delays. When added together, the resulting signal's amplitude, phase, and angle of arrival fluctuate over time. This effect is termed as multipath fading, and the wireless propagation channel is called the fading channel [22].

2.1.1 Mathematical Model

A signal received via a fading channel is assumed to be corrupted by channel fading and additive noise. Mathematically, it is generally described in terms of a transmitted signal $s(t)$, convolved with the impulse response of the channel $h_c(t)$, added to an additive noise source $n(t)$. Thus, the received signal, $r(t)$, can be written as [2]

$$r(t) = s(t) * h_c(t) + n(t) \tag{2.1}$$

where $*$ denotes convolution. In the case of a wireless propagation environment, $h_c(t)$ can be partitioned in terms of two random variables [22]

$$h_c(t) = m(t) \times r_0(t) \tag{2.2}$$

where $m(t)$ is called the large-scale fading component, and $r_0(t)$ is called the small-scale fading component.

Large-scale fading, $m(t)$, represents the average signal power attenuation or the path loss due to motion over large areas. Both theoretical and measurement-based models indicate that $m(t)$ has a log-normal probability density function (pdf), i.e., the magnitude of $m(t)$ measured in decibels has a Gaussian pdf. Small-scale fading, $r_0(t)$, represents the fluctuation of the received signal over a relatively smaller travel distance or a short time interval when the signal power has the same local mean.

2.1.2 Small-Scale Fading

Small-scale fading can be categorized into frequency-selective fading and flat fading from the point of view of time-spreading, or can be classified into fast fading and slow fading depending on its time-variant behaviour [22, Ch. 18].

Time-spreading can be characterized in both the time-delay domain and the frequency domain. In the time-delay domain, it is characterized as a multipath delay spread, τ. It reflects the fading channel's non-optimum impulse response. That is, if we transmit an extremely short pulse, ideally an impulse, over a multipath channel, the received signal would appear as a train of pulses. In the frequency domain, time-spreading can be characterized as a channel coherent bandwidth, $(\Delta f)_c$. It occurs if the modulation bandwidth exceeds the coherent bandwidth of the channel. Time-spreading partitions the small-scale fading in the following manner. When a signal is transmitted through the channel, if $(\Delta f)_c$ is small in comparison to the bandwidth of the transmitted signal, the channel is said to be frequency-selective. On the other hand, if $(\Delta f)_c$ is large in comparison to the bandwidth of the transmitted signal, the channel can be viewed as frequency-nonselective or flat, and the delay spread is negligible. Frequency-selective fading causes intersymbol interference (ISI), which can be compensated for by equalization techniques [2, Ch. 10].

The time-variant behaviour of the channel results from the antenna's motion or spatial changes. As a result of such time variations, the nature of the multipath fading varies over time. That is, if we transmit the same pulse over and over, we will observe changes in the received pulse train, including changes in the size of the individual pulses, changes in the time delays, and changes in the number of pulses observed. In the time domain, this behaviour can be characterized as a coherence time, $(\Delta t)_c$, while in the Doppler-shift domain, it can be characterized as a channel fading rate of Doppler spread, f_D. If $(\Delta t)_c$ is smaller than the time duration of a transmission symbol, the channel is said to be fast fading. Otherwise, a channel is referred to as introducing slow fading, and the effects of Doppler spread are negligible at the receiver. While equalization is used to fight ISI, diversity is usually employed to reduce the depth and duration of fast fading.

2.1.3 Rayleigh Fading

In small-scale fading, if the multiple reflective paths are large in number and there is no line-of-sight signal between the transmitter and receiver antennas, the envelope of the received signal is Rayleigh distributed with pdf [22]

$$p(r) = \frac{r}{\sigma_r^2} e^{-r^2/2\sigma_r^2}, \quad r \geq 0 \tag{2.3}$$

where r is the envelope amplitude of the received signal, and $2\sigma_r^2$ is the mean power of the multipath signal. The phase of the received signal is assumed to be uniformly distributed in the interval $(0, 2\pi)$. In this case, the environment is said to be in Rayleigh fading. Rayleigh fading is frequently used to describe the statistical time varying nature of the received signal envelope of a flat faded signal. Occurring primarily in the ultra-high-frequency (UHF) band (300 MHz-3 GHz), it affects mobile systems such as cellular and personal communication systems (PCS).

2.2 Diversity Schemes

Diversity techniques have been used for decades and are well-known methods for combating the effects of fading in wireless communication systems. Diversity is implemented by sending or receiving the same information signal over two or more independent (or at least highly uncorrelated) radio paths. If one radio path undergoes a deep fading, another independent path may have a strong signal. If the signals from these transmission paths are properly combined, both the instantaneous and average signal-to-noise ratios (SNRs) of the resulting signal may be improved, often by as much as 20 dB to 30 dB [23]. Thus, diversity reduces the severity of fading and improves the reliability of transmission.

2.2.1 Microscopic Diversity and Macroscopic Diversity

As discussed in Section 2.1, there are two types of fading, small-scale fading and large-scale fading. The diversity methods used to combat these two categories of fading are termed microscopic diversity and macroscopic diversity techniques, respectively [23].

Small-scale fading, which is characterized by deep and rapid amplitude fluctuations, occurs when a mobile user moves over distances of just a few wavelengths. Microscopic diversity techniques can exploit these rapidly changing signals to prevent deep fades from occurring. For example, if two antennas separated by a fraction of a meter are used in a mobile, while one receives a null, the other may receive a strong signal; by selecting the stronger antenna, the mobile can improve substantially the average SNR on the forward link.

As large-scale fading is caused by shadowing over large areas, macroscopic diversity takes advantage of the large separations between the serving base stations. It can improve system performance in both the reverse link and the forward link. For example, the mobile can select a base station which is not shadowed when others are in order to receive signals from a better forward link. Another example is that, if base station antennas are sufficiently separated in space, the base station is also able to improve the reverse link by selecting the antenna with the strongest signal from the mobile.

2.2.2 Receiver Diversity and Transmitter Diversity

Multiple antennas, either at the transmitter side, the receiver side, or both, have been used to increase diversity to combat channel fading. Under the assumption that each pair of transmit and receive antennas provides an independent signal path from the transmitter to the receiver, these independent faded paths are unlikely to all be in a deep fade, i.e., strongly distorted, simultaneously. Thus an improved signal may be obtained by forming a weighted combination of the received copies or by selecting the strongest received signals.

The traditional approach for diversity is to use multiple antennas at the receiver end. Since the use of radio frequency chains (or selection and switching circuits) in multiple antennas increases the size and the cost of the remote units and given that there are restrictions on the processing power available at remote units, receive diversity has almost exclusively been implemented at base stations to improve their reception quality (i.e., in the uplink). Clearly, a base station that employs receiver diversity can improve the quality

of the uplink (from the mobile to the base station) without adding any additional cost, size or power consumption to the mobile.

The development of transmit diversity techniques started in the early 1990's and since then the interest in the topic has grown in a rapid fashion. In transmit diversity, a receiver branch receives the sum of faded signals from all transmitter antennas. In order to achieve a better diversity order, different transmission methods have to be applied, e.g., delay diversity, space-time trellis codes, or space-time block codes, etc. This makes a transmitter diversity system more complicated than a receiver diversity system. Recently, there is increasing interest in transmitter diversity to realize similar performance benefits in the downlink. This is attractive because a performance increase is possible without adding extra antennas, power consumption or significant complexity to the mobile. Also, the cost of the extra transmit antennas at the base station can be shared among all users.

2.2.3 Diversity Classifications

Diversity exploits the random nature of radio propagation by finding independent signal paths for communications. There are several techniques for obtaining diversity branches. This section provides a brief introduction to space, polarization, angle, frequency, and time diversity [24].

2.2.3.1 Space Diversity

In space diversity, the distance between the antennas is made large enough to ensure independent fading. At the mobile, a spacing of half of a wavelength between antennas is sufficient. However, since the important scatterers are generally on the ground in the vicinity of the mobile, the base station antennas must be spaced considerably farther apart to achieve decorrelation. Usually, a separation on the order of several tens of wavelengths is required at the base station. Because it is relatively simple to implement, space diversity is a widely used method in both past and present wireless communications systems.

2.2.3.2 Polarization Diversity

Polarization diversity can be considered as a special case of space diversity. It utilizes two orthogonally polarized waves – a horizontally polarized wave and a vertically polarized wave. When both waves are transmitted simultaneously, the received signals will exhibit uncorrelated fading statistics. However, only two diversity branches are available since there are only two orthogonal polarizations.

2.2.3.3 Angle Diversity

Since the received signal arrives at the antenna via several paths, each with a different angle of arrival, the signal component can be isolated by using directional antennas. Each directional antenna will isolate a different angular component. Hence, the signals received from different directional antennas pointing at different angles are uncorrelated.

2.2.3.4 Frequency Diversity

Frequency diversity uses sufficiently spaced carrier frequencies to provide the uncorrelated transmission paths. The coherence bandwidth provides the means to determine the required frequency spacing. When frequency separations are in excess of more than several times the coherence bandwidth, the signal fadings will be essentially uncorrelated.

2.2.3.5 Time Diversity

Time diversity generates independent paths in the time domain. When the same data are sent over a fixed channel at different times, the received signals can be uncorrelated if the time separations are large enough. The required time separation is at least as great as the reciprocal of the fading bandwidth, which is twice the speed of the mobile station divided by the wavelength. For a mobile station, time diversity offers little advantage, in contrast to all of the other diversity types discussed above, because the benefit depends on the speed of the mobile station.

2.3 Combining Techniques

When independent transmission paths are generated, a receiver needs to properly combine the signals from these paths in order to improve the signal quality. In this section, we describe several diversity combining methods, selection combining (SC), switch-and-stay combining (SSC), maximal ratio combining (MRC), equal gain combining (EGC), and generalized selection combining (GSC).

2.3.1 Selection Combining

Selection combining [24] is the simplest method of all. In selection combining, only one receiver branch, the one with the highest instantaneous SNR, is connected to the demodulator. In practice, the branch with the largest signal-plus-noise is normally used, since it is difficult or expensive to measure SNR, especially for a high signalling rate. Practically, SNR selection circuitry cannot function on a truly instantaneous basis but has to be designed to work on internal time constants shorter than the reciprocal of the signal fading rate.

2.3.2 Switch-and-Stay Combining

Switch-and-stay combining [24], [25] is very similar to selection diversity except that instead of always using the best receiver branch, all branches are scanned in a fixed sequence until one is found to be above a predetermined threshold. The received signal on this branch is then selected and monitored. If it falls below the threshold, the scanning process is again initiated. It has simpler implementation as it does not require continuous monitoring on all the receiver branches, but it offers poorer performance than selection combining.

2.3.3 Maximal Ratio Combining

In maximal ratio combining [24], the received signals from all antennas are first co-phased, then weighted proportionately in terms of their signal-voltage-to-noise-power ratios, and

finally summed. In this way, an output SNR equal to the sum of the individual SNRs from each receiver branch is provided. This technique gives the best statistical reduction of fading among any known linear combining techniques.

2.3.4 Equal Gain Combining

Equal gain combining is similar to maximal ratio combining as the signals from all receiver branches are also co-phased [24]. However, the co-phased signals are combined without being weighted. In practice, this scheme is useful when it is not convenient to provide weighting coefficients or when modulation techniques have equal energy symbols. The performance is only marginally inferior to that of maximal ratio combining and is superior to that of selection combining.

2.3.5 Generalized Selection Combining

Generalized selection combining was proposed to overcome the disadvantages of the four above selection combining schemes. It combines two techniques, MRC/EGC and SC together [26]. It adaptively selects the strongest (highest SNR) paths among the available ones and combines them together by using MRC or EGC. This scheme offers less complexity than that of the conventional MRC/EGC receivers since it has a fixed number of receiver branches independent of the number of multipaths. Moreover, GSC receivers are expected to be more robust with respect to channel estimation errors since the weakest SNR paths (and hence the ones which are the most exposed to these errors) are excluded from the combining process. However, its better performance over SC comes at a cost of increased receiver complexity and power consumption.

2.4 Selection Combining Schemes

The simplest combining scheme, selection combining, is the main focus in this thesis. In general, MIMO antenna selection combining includes receiver antenna selection, transmit-

ter antenna selection and joint Tx/Rx selection. Both Tx/Rx selection and Tx selection require that channel estimation be fed back from the receiver to the transmitter. In order to avoid the need for a feedback channel, and to keep the system simple, some systems will implement Rx selection diversity only. In MIMO Rx selection diversity, L_s out of L Rx antennas are selected while the Tx uses all available antennas.

Conventionally, selection combining selects the receiver branch providing the largest SNR. However, some other selection combining schemes have been proposed recently. In this section, four selection schemes are considered, SNR selection, $S+N$ selection, $|ar|$ selection, and $|aw|$ selection.

2.4.1 SNR Selection

The traditional selection rule for a selection combining system is based on SNR. When a selection takes place at the receiver side, the branch providing the largest SNR is selected for data recovery out of L diversity branches. For BPSK signalling in a Rayleigh fading, the traditional selection combining model is given in [27] and the BER expression is [28]

$$P_b = \frac{1}{2} \cdot \sum_{k=0}^{L} (-1)^k \cdot \binom{L}{k} \cdot \sqrt{\frac{\bar{\gamma}_b}{\bar{\gamma}_b + k}} \tag{2.4}$$

where $\bar{\gamma}_b$ is the average SNR per bit.

Note that the BER is computed by averaging the time-invariant (static) channel-error rate $P(\gamma)$ over the probability density function $f(\gamma)$ of the largest instantaneous SNR [29]. This method is appropriate only if, in measuring the largest SNR, the average noise power is taken over a sufficiently long time, τ, such that it may be considered as a constant across all branches [28].

2.4.2 $S+N$ Selection

The conventional selection combining scheme selects, among the L diversity branches, the branch providing the largest signal-to-noise ratio (or largest fading amplitude). However,

in practical implementations, the measurement of SNR may be difficult or expensive, especially for high signalling rates. For this reason, the branch with the largest signal-plus-noise is often chosen. We use $S+N$ to denote a signal-plus-noise sample.

The system model for BPSK with $S+N$ selection diversity combining is shown in [28, Fig. 7]. In this selection, signals from all the receiver branches are first co-phased, then the one with the largest real part amplitude is chosen to be detected. The BER expression is [28]

$$P_b = \int_{-\infty}^{0} \left\{ \int_0^{\infty} \frac{1}{\sigma\sqrt{2\pi}} e^{-(x_1-2\alpha_1)^2/2\sigma^2} \cdot 2\alpha_1 e^{-\alpha_1^2} d\alpha_1 \right\} \cdot \left\{ \int_0^{\infty} \left[Q\left(\frac{x_1+2\alpha_j}{\sigma}\right) + Q\left(\frac{x_1-2\alpha_j}{\sigma}\right) - 1 \right] \cdot 2\alpha_f e^{-\alpha_j^2} d\alpha_j \right\}^{L-1} dx_1 \tag{2.5}$$

where $\sigma^2 = 2/\bar{\gamma}_b$, and $\bar{\gamma}_b$ is the average SNR per bit. The expression (2.5) can be evaluated numerically.

2.4.3 $|ar|$ Selection

The $|ar|$ selection scheme was first proposed in [30] for a system with 1 Tx antenna and L receiver antennas. The selection rule is to choose the receiver branch with the largest log-likelihood ratio (LLR). The basic system model is described as follows. The lowpass equivalent received signal at the ith branch before phase compensation is

$$\omega_i = a_i e^{j\phi_i} \cdot x + n_i \quad i = 1,2,\cdots,L \tag{2.6}$$

where a_i is the fading amplitude in the ith branch, ϕ_i is the fading phase in the ith branch, x represents the BPSK signalling, and n_i is the additive complex Gaussian noise in the ith branch. After phase compensation, the received signal becomes

$$r_i = \mathrm{Re}\{\omega_i e^{-j\phi_i}\} = a_i \cdot x + \eta_i, \quad i = 1,2,\cdots,L \tag{2.7}$$

where $\eta_i = \mathrm{Re}\{n_i e^{-j\phi_i}\}$. Then, the LLR Λ_i in the ith branch is given by

$$\begin{aligned}\Lambda_i &= \ln\frac{\Pr\left(x=\sqrt{E_b}|a_i,\phi,\omega_i\right)}{\Pr\left(x=-\sqrt{E_b}|a_i,\phi,\omega_i\right)} \\ &= \ln\frac{\Pr\left(\omega_i|a_i,\phi,x=\sqrt{E_b}\right)}{\Pr\left(\omega_i|a_i,\phi,x=-\sqrt{E_b}\right)} \\ &= \ln\frac{\exp\left\{-\left|\omega_i - a_i e^{j\phi_i}\sqrt{E_b}\right|^2/N_0\right\}}{\exp\left\{-\left|\omega_i + a_i e^{j\phi_i}\sqrt{E_b}\right|^2/N_0\right\}} \\ &= \frac{4\sqrt{E_b}}{N_0}a_i\mathrm{Re}\left\{\omega_i e^{-j\phi_i}\right\} = \frac{4\sqrt{E_b}}{N_0}a_i r_i.\end{aligned} \tag{2.8}$$

The receiver branch which provides the largest $|a_i r_i|$ is chosen to be detected and the sign of the $a_i r_i$ is the hard decision data value. This selection combining is, therefore, referred to as $|ar|$-selection.

The closed-form BER expression is [30]

$$\begin{aligned}P_b = & L\frac{1}{\left(\sqrt{2(1+\bar{\gamma}_b)}\right)^L}\sum_{k=0}^{L-1}\binom{L-1}{k} \\ & \cdot\left\{\sum_{l=0}^{k}\sum_{m=0}^{L-1-k}\binom{k}{l}\binom{L-1-k}{m}(-1)^{l+m}\frac{1}{\alpha(l+1)+\beta m}\right\}\end{aligned} \tag{2.9a}$$

where

$$\alpha = \sqrt{2}\left(\sqrt{1+\bar{\gamma}_b}+\sqrt{\bar{\gamma}_b}\right) \tag{2.9b}$$

$$\beta = \sqrt{2}\left(\sqrt{1+\bar{\gamma}_b}-\sqrt{\bar{\gamma}_b}\right). \tag{2.9c}$$

2.4.4 $|a\omega|$ Selection

Based on ar-selection, another simpler selection scheme, $|a\omega|$-selection, was also proposed in [30]. $|a\omega|$-selection selects the branch providing the largest $|a_i\omega_i|$. It does not require phase information in the branch selection process and thus substantially reduces implementation complexity. The BER performance however is poorer than that of $|ar|$ selection.

2.5 Comparisons of Selection Combining Schemes

Fig. 2.1 shows the BER performance versus SNR for the four selection combining schemes in a flat Rayleigh fading with $L = 2$ and $L = 4$. For comparison, the BER performance of MRC is also shown here.

Several interesting observations can be made from Fig. 2.1. First, when $L = 2$, MRC and $|ar|$-selection have the same performance, but when $L = 4$, MRC outperforms $|ar|$-selection by about 0.5 dB. Second, for both 2-fold and 4-fold diversity, $|ar|$-selection outperforms $|aw|$-selection, $|aw|$-selection outperforms $S+N$ selection, and $S+N$ selection outperforms *SNR*-selection. Third, while for $L = 2$, $|aw|$-selection only shows a slightly better performance than $S+N$ selection, for $L = 4$, it shows power gains of 0.5 dB over $S+N$ selection and 1.7 dB over *SNR*-selection diversity systems. Fourth, for all selection schemes, the power gain increases with increasing L, as expected.

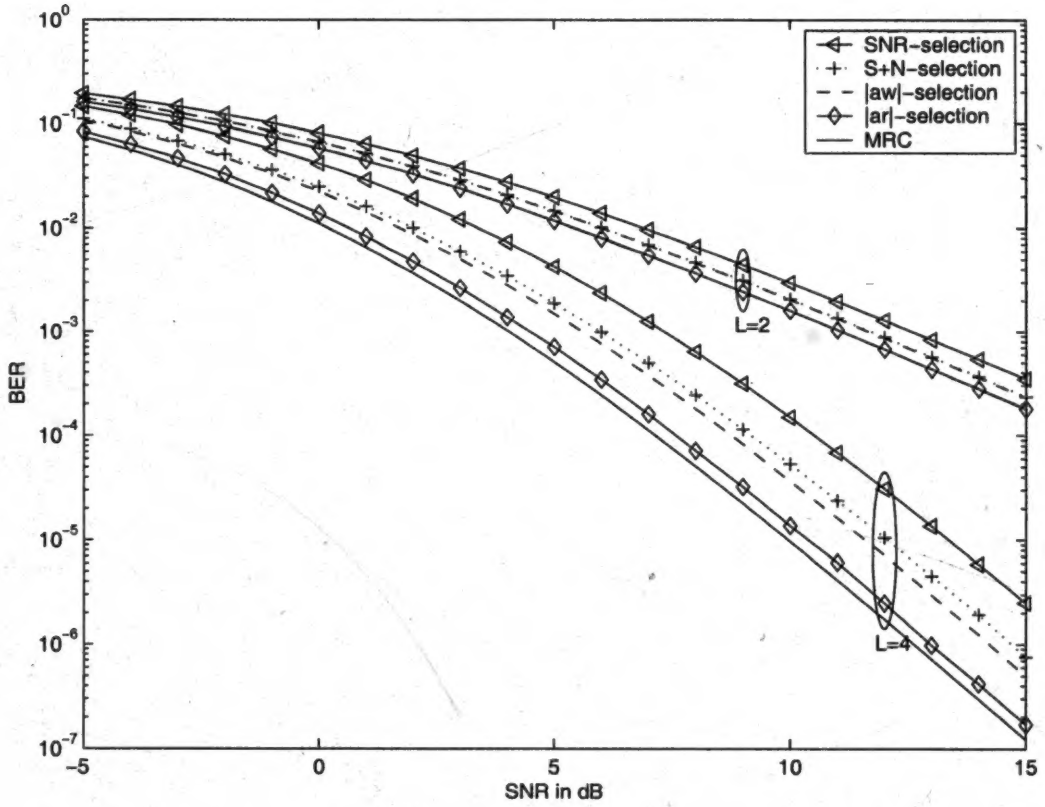

Fig. 2.1. The BER versus SNR for four selection combining schemes and MRC.

Chapter 3

Space-Time System and Channel Estimation Error

The design of a wireless system requires trading-off several different aspects. These include bandwidth efficiency, data rate, network capacity, quality of service, and cost, etc. Space-time (ST) wireless communications, which uses multiple antennas at the transmitter and receiver in a wireless system, is a promising technology that can significantly improve these measures.

This chapter first gives an introduction to space-time systems, including the system structure and specialized coding techniques in Section 3.1. As one type of space-time system, the Alamouti system is illustrated in Section 3.2. It is the simplest ST system which requires only two transmit antennas. It is simple as it requires no feedback from the receiver to the transmitter, and no bandwidth expansion if the diversity is achieved in space but not in time or in frequency.

In the Alamouti diversity system, channel estimation is needed before a space-time combiner (see Fig. 3.2). That is, the performance of the Alamouti system relies on the accuracy of channel estimation. Hence, an introduction to channel estimation error is given in Section 3.3 and a detailed derivation of channel estimation error for the Alamouti system is given in Section 3.4.

3.1 Space-Time Wireless Communication Systems

3.1.1 Introduction

The use of multiple antennas goes back to Marconi and the early radio pioneers. It became an active research area during and after World War II in radar systems. With the development of digital signal processing in 1970s, started more sophisticated applications in the military. Along with several new proposals for using antennas to increase wireless link capacity, the research done at Bell Labs began a new revolution in information and communications theory in the mid 1990s. Now the research related to ST systems has become an important topic and a lot of work has been done in this area.

Space-time systems improve wireless communication in terms of improving the received SNR and increasing the data capacity. The utilization of multiple antennas exploits the multiple paths between transmitter and receiver antennas. With this increased diversity, the combined SNR is improved at the receiver side. If the channel between each transmit-receive antenna pair fades independently, the diversity order is equal to the product of the number of transmitter and receiver antennas, i.e., $L_t L_r$. On the other hand, in a wireless fading channel with sufficiently rich scattering, space-time systems can achieve capacities that were unthinkable even a decade ago. That is, when the wireless channel has a sufficient number of degrees of freedom, the data streams transmitted from multiple transmitter antennas can be separated, thus leading to parallel data paths. The resultant capacity of the radio channel grows with $\min(L_t, L_r)$, i.e., linearly with the number of antennas.

3.1.2 Antenna Configurations

There are several different antenna configurations for ST systems. A SISO system is the simplest and most familiar configuration. A single-input and multiple-output (SIMO) system has a single transmitter antenna and multiple receiver antennas. A multiple-input single-output (MISO) system has multiple transmitter antennas and a single receiver antenna. A MIMO system has multiple antennas at both receiver and transmitter sides. The

MIMO multiuser (MIMO-MU) configuration refers to the case where a base-station with multiple antennas communicates with P users each with one or more antennas.

3.1.3 Space-Time System Structure

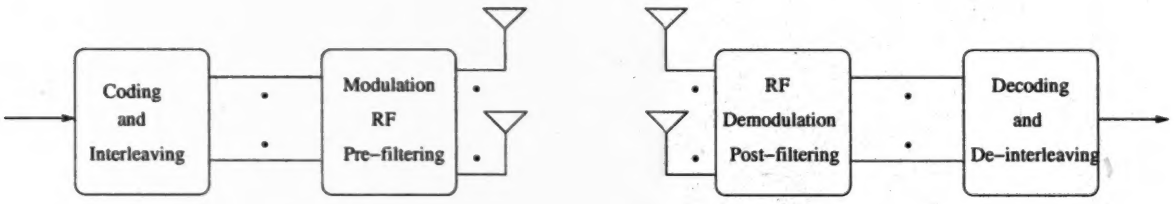

Fig. 3.1. A space-time wireless communication system.

Fig. 3.1 shows a typical ST wireless system with L_t transmitter antennas and L_r receiver antennas. The input data bits first enter a space-time encoder that inserts parity bits into the data stream. These parity bits function as protection against noise and also capture diversity from space and possibly frequency or time dimensions in a fading environment. After being encoded, the bits are interleaved across space, time, and frequency into L_t symbol streams. The symbol streams are then pre-filtered, modulated, and then transmitted from L_t antennas.

After being distorted by the fading channel, these transmitted signals arrive at the L_r receiver antennas. The RF chains at the receiver corrupt the received signals with additive thermal noise. Then the mixture of signal plus noise is matched-filtered and sampled to produce L_r output streams. Some form of additional post-filtering may also be applied. These streams are then deinterleaved and decoded to produce the output data bits.

The difference between a ST wireless system and a conventional system is that a ST wireless system uses multiple antennas, ST encoding and interleaving, ST pre-filtering and post-filtering, and ST decoding and deinterleaving.

3.1.4 Space-Time Coding

Using only receiver diversity, e.g., in a SIMO system, since receivers can estimate the channel and implement MRC, it is possible to achieve a diversity of order L_r. However, with transmitter diversity, e.g., in a MISO system, it is more complicated to achieve the same diversity order.

If we assume that transmitters know the channel, the transmitted signals can be pre-weighted according to their transmission path strength. In this way, it is still possible to achieve an error probability the same as in a SIMO system with MRC. However, if we assume that there is no channel knowledge at the transmitter, diversity cannot be achieved if only one time interval is used to transmit a single symbol, i.e., no space-time coding is involved. This can be solved when we use two time intervals to transmit a single symbol, where in the first interval only the first antenna is used and where during the second time interval only the second antenna is used, the error rate associated with this method is equal to that for the case where we have one transmit and two receive antennas. This simple example shows how transmitter diversity is achieved by using space-time coding. However, the data rate is halved. In practice, space-time coding is concerned with the harder and more interesting question. How can we maximize the transmitted information rate, at the same time that the error probability is minimized.

There are two types of ST diversity code, space-time trellis codes (STTCs) and space-time block codes (STBCs). Both codings combine signal processing at the receiver with coding techniques appropriate to multiple transmit antennas.

STTCs are an extension to conventional trellis codes to multi-antenna systems. Each STTC can be described using a trellis. The encoder output has L_t components corresponding to the symbols to be transmitted over L_t transmitter antennas. Specific STTCs designed for 2/4 transmitter/receiver antennas perform extremely well in slow fading environments and come close to the outage capacity [31]. However, when the number of transmitter antennas is fixed, the decoding complexity of a STTC increases exponentially with the transmission rate [32].

STBCs are an extension of block codes to multiple antenna systems. STBCs are attractive due to their low implementation and decoding complexity despite their performance penalty compared to STTCs. STBCs will be outperformed by STTCs designed to optimize the rank and determinant criteria. However, STBCs concatenated with standard AWGN codes can outperform some of the best-known STTCs in terms of error rate performance. The simplest STBC is the Alamouti scheme.

3.2 Alamouti Scheme

As the simplest STBC, the Alamouti scheme is much less complex than a STTC for two transmitter antennas. Alamouti gave the system model for this two transmitter antenna diversity in [1], with both one receiver and two receivers in the system as examples. The system can be easily generalized to include L receiver antennas by using the combining or selection schemes mentioned in Chapter 2. In this section, we will briefly go through this system model. The system structure for the special case of one receiver antenna is shown in Fig. 3.2 .

The Alamouti scheme is defined by the following three functions [1], the encoding and transmission sequence of information symbols at the transmitter, the combining scheme at the receiver, and the decision rule for maximum-likelihood detection.

3.2.1 The Encoding and Transmission Sequence

Signals s_1 and s_2, corresponding to two information symbols, are sent simultaneously during two consecutive symbol intervals. At the first symbol interval, s_1 is transmitted from antenna 1 and s_2 is transmitted from antenna 2. During the next symbol period, signal $-s_2^*$ is transmitted from antenna one, and signal s_1^* is transmitted from antenna two, where * denotes the complex conjugate operation. In this thesis, BPSK modulation is assumed so that the transmitted signal is either $+1$ or -1. The encoding may also be done in space and frequency. That is, instead of two adjacent symbol periods, two adjacent carriers may be

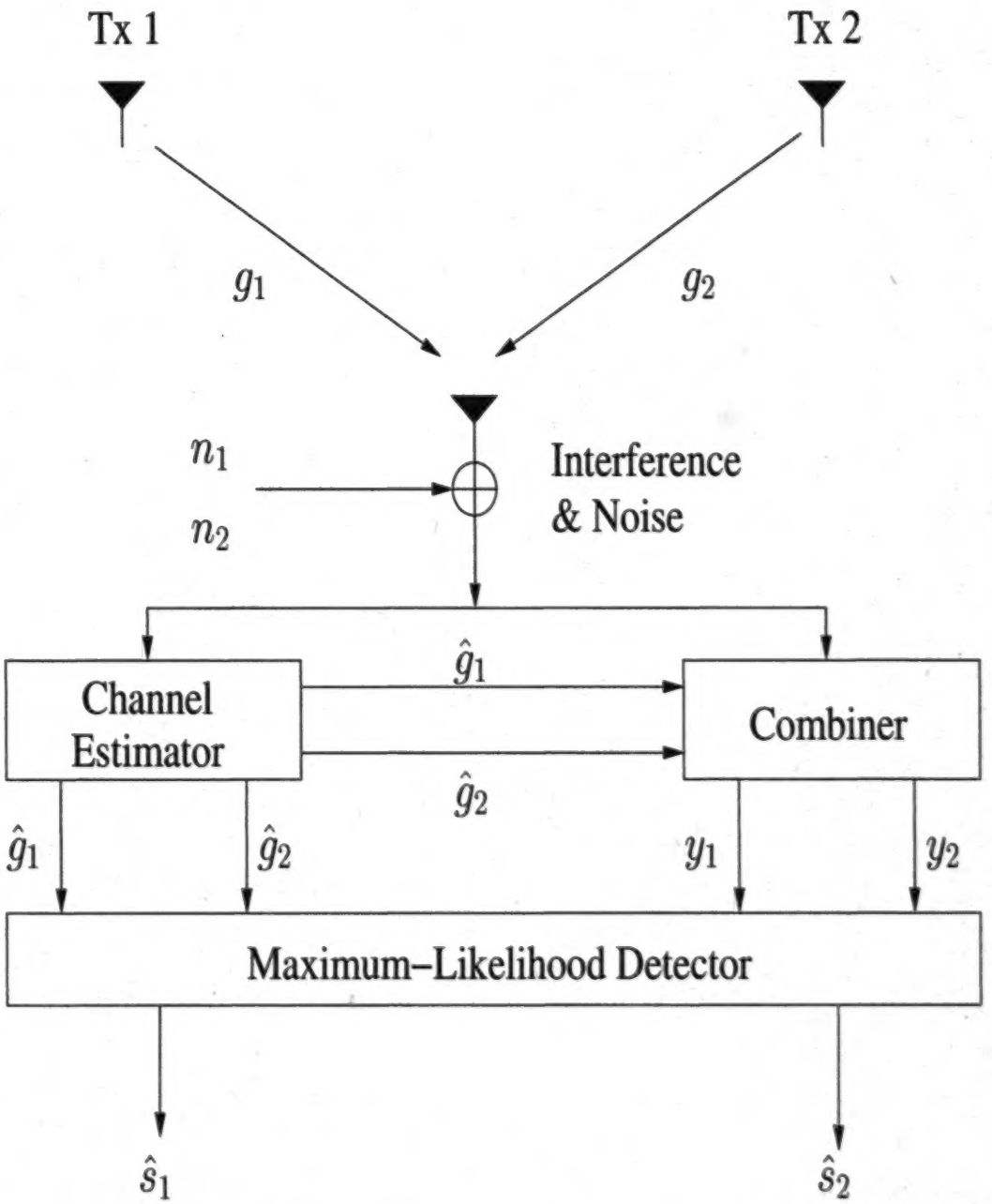

Fig. 3.2. The Alamouti system with two transmitter antennas and one receiver antenna (after [1, Fig. 2]).

used (space frequency coding).

The channel is assumed constant across two consecutive symbols and is modeled as a complex Gaussian process. With $g_{1,i}$ denoting the complex channel gain between the 1st transmit antenna and the ith receive antenna, and $g_{2,i}$ representing the complex channel gain between the 2nd transmit antenna and the ith receive antenna, the corresponding received signals in these two intervals on the ith branch can be expressed as [1]

$$\begin{aligned} r_{1,i} &= g_{1,i}s_1 + g_{2,i}s_2 + n_{1,i} \\ r_{2,i} &= -g_{1,i}s_2^* + g_{2,i}s_1^* + n_{2,i}, \quad i = 1,2\cdots,L \end{aligned} \tag{3.1}$$

where $n_{1,i}$ and $n_{2,i}$ are complex random variables representing receiver noise and interference. Both $g_{j,i}$ and $n_{j,i}$, $j = 1,2$ are assumed to be Gaussian random variables with variances σ_g^2 and σ_n^2 in the real and imaginary part, respectively. For BPSK, the average SNR of the received signal is defined here as $\bar{\gamma}_b = \frac{2\sigma_g^2}{\sigma_n^2}$.

3.2.2 The Combining Scheme

The combiner shown in Fig. 3.2 builds the following two combined signals that are sent to the maximum-likelihood detector

$$\begin{aligned} y_{1,i} &= \hat{g}_{1,i}^* r_{1,i} + \hat{g}_{2,i} r_{2,i}^* \\ y_{2,i} &= \hat{g}_{2,i}^* r_{1,i} - \hat{g}_{1,i} r_{2,i}^* \end{aligned} \tag{3.2}$$

where $\hat{g}_{1,i}$ and $\hat{g}_{2,i}$ denote the estimates of fading gains $g_{1,i}$ and $g_{2,i}$. They are estimated at the receiver prior to space-time combining.

3.2.3 The Decision Rule

These combined signals are then sent to the maximum-likelihood decoder, which uses the decision criteria $\hat{s}_j = \text{sgn}(\text{Re}(y_{j,i}))$, $j = 1,2$, where $\hat{s}_j$ represents the estimation of s_j and

$\text{sgn}(x) = \text{signum}(x)$ is defined as

$$\text{sgn}(x) = \begin{cases} 1, & \text{if } x > 0 \\ 0, & \text{if } x = 0 \\ -1, & \text{if } x < 0. \end{cases}$$

3.3 Fading Estimation Error

The fading estimate $\hat{g}_{j,i}$ cannot be exactly the same as the channel fading gain $g_{j,i}$ because it is extracted from fading corrupted signals. The difference between the channel fading gain and its estimate is defined as fading gain estimation error and is assumed to be a Gaussian error in [33]. This error is due to either an inaccurate estimation method or the decorrelation of the fading distortion at the time of estimation compared to the time of application in recovering the data symbol.

Same as in [33], we assume here identical statistics for the independent diversity branches, and that the correlation between $g_{j,i}$ and its estimate $\hat{g}_{j,i}$ is the same on each branch. As the work in [33] only assumes that the variance of the channel gain on all branches is equal to that of its estimate, it is extended here to include the case when the variances of the channel gain and its estimate are unequal. We define

$$g_{j,i} = \left(\frac{R_c}{\sigma_{\hat{g}}^2} + j \frac{R_{cs}}{\sigma_{\hat{g}}^2} \right) \hat{g}_{j,i} + d_{j,i} \tag{3.3}$$

where $d_{j,i}$ is a Gaussian error uncorrelated with $\hat{g}_{j,i}$. The parameters R_c and R_{cs} are given by

$$R_c = E[g_I \hat{g}_I] = E[g_Q \hat{g}_Q] \tag{3.4a}$$

$$R_{cs} = E[g_I \hat{g}_Q] = -E[g_Q \hat{g}_I]. \tag{3.4b}$$

Under the Rayleigh fading assumption, $R_{cs} = 0$ [34], and we can simplify (3.3) to

$$g_{j,i} = b\hat{g}_{j,i} + d_{j,i} \tag{3.5}$$

where $b = \frac{R_c}{\sigma_{\hat{g}}^2}$. The variance of the real (or imaginary) component of $d_{j,i}$ is $\sigma_d^2 = (1-\rho)\sigma_g^2$ [35], where ρ is the squared amplitude of the cross-correlation coefficient of the channel fading and its estimate

$$\rho = \frac{E^2[g\hat{g}^*]}{E[|g|^2]E[|\hat{g}|^2]} = \frac{R_c^2}{\sigma_g^2\sigma_{\hat{g}}^2} = \frac{\sigma_{\hat{g}}^2}{\sigma_g^2}b^2. \tag{3.6}$$

It is commonly used to measure the level of channel estimation error.

3.4 Channel Estimation Error for Pilot Symbol Assisted Modulation in an Alamouti System

Pilot symbol assisted modulation has proved to be effective to estimate the fading channel gain. In this section, a detailed description of channel estimation error for PSAM is given. The squared cross-correlation coefficient of the channel fading and its estimate, ρ, for PSAM in an Alamouti system is derived. Since ρ in (3.6) is a function of R_c and $\sigma_{\hat{g}}^2$, R_c and $\sigma_{\hat{g}}^2$ are derived first before the final expression of ρ is given.

3.4.1 Fading Estimation in PSAM

We assume that PSAM is used for channel estimation. The PSAM frame format is similar to that considered in [36, fig. 2], where pilot symbols are inserted periodically into the data sequence. Since there are two receiver antennas and an Alamouti scheme is employed, the estimation of channel state information takes at least two symbol intervals and the channel state must remain constant over that period. Therefore, we assume that the fading gain remains constant over two consecutive symbol intervals. Under this assumption, two consecutive pilot symbols are transmitted together between data symbols; $\frac{N}{2}$ clusters, each with 2 symbols, are formatted into one frame of N symbols, where N is an even number, with the first two pilot symbols ($n = 0$) followed by $N-2$ data symbols ($1 \leq n \leq N/2-1$). The composite signal is transmitted over $2L$ flat, Rayleigh fading channels. At the receiver,

after matched-filter detection, the pilot symbols are extracted and interpolated to form an estimate of the channel in the following manner.

Rewrite (3.1) to include the above assumptions for BPSK as

$$r^n_{1,i,k} = g^n_{1,i,k}s_1 + g^n_{2,i,k}s_2 + n^n_{1,i,k} \tag{3.7a}$$

$$r^n_{2,i,k} = -g^n_{1,i,k}s_2 + g^n_{2,i,k}s_1 + n^n_{2,i,k} \tag{3.7b}$$

where $r^n_{j,i,k}, j = 1,2$ denotes the jst received symbol at the nth symbol cluster of the kth data frame in the ith receiver branch, $n^n_{j,i,k}, j = 1,2$ denotes the additive noise for the jst symbol interval at the nth symbol cluster of the kth data frame in the ith receiver branch, and $g^n_{j,i,k}, j = 1,2$ denotes the fading gain between the jth transmitter antenna and the ith receiver antenna at the nth symbol cluster of the kth data frame. Since the pilot symbols are known to the receiver, without loss of generality, we assume that the two pilot symbols in the first cluster ($n = 0$) of the frame have the values $+1$ and -1, respectively. Then for the two received pilot symbols, (3.7a) becomes

$$r^0_{1,i,k} = g^0_{1,i,k} - g^0_{2,i,k} + n^0_{1,i,k} \tag{3.8a}$$

$$r^0_{2,i,k} = g^0_{1,i,k} + g^0_{2,i,k} + n^0_{2,i,k}. \tag{3.8b}$$

Averaging (3.8a) and (3.8b) , we obtain the estimate of $g^0_{1,i,k}$ as

$$\hat{g}^0_{1,i,k} = g^0_{1,i,k} + \frac{n^0_{1,i,k} + n^0_{2,i,k}}{2}. \tag{3.9a}$$

Subtracting (3.8a) from (3.8b) generates

$$\hat{g}^0_{2,i,k} = g^0_{2,i,k} + \frac{n^0_{2,i,k} - n^0_{1,i,k}}{2}. \tag{3.9b}$$

The fading at the nth symbol ($1 \le n \le N/2 - 1$) in the kth frame of the ith branch is estimated from $2K$ pilot symbols of K adjacent frames with pilot symbols from $-\lfloor \frac{K-1}{2} \rfloor$ previous frames and from $\lfloor \frac{K}{2} \rfloor$ subsequent frames. These estimates are given by

$$\hat{g}^n_{1,i,k} = \sum_{k=-\lfloor \frac{K-1}{2} \rfloor}^{\lfloor \frac{K}{2} \rfloor} h^n_k \hat{g}^0_{1,i,k} = \sum_{k=-\lfloor \frac{K-1}{2} \rfloor}^{\lfloor \frac{K}{2} \rfloor} h^n_k \left(g^0_{1,i,k} + \frac{n^0_{1,i,k} + n^0_{2,i,k}}{2} \right) \tag{3.10a}$$

$$\hat{g}^n_{2,i,k} = \sum_{k=-\lfloor \frac{K-1}{2} \rfloor}^{\lfloor \frac{K}{2} \rfloor} h^n_k \hat{g}^0_{2,i,k} = \sum_{k=-\lfloor \frac{K-1}{2} \rfloor}^{\lfloor \frac{K}{2} \rfloor} h^n_k \left(g^0_{2,i,k} + \frac{n^0_{2,i,k} - n^0_{1,i,k}}{2} \right), \quad n = 1, \cdots \frac{N}{2} - 1 \tag{3.10b}$$

where h^n_k is the interpolation coefficient for the nth data symbol in the kth frame.

3.4.2 Derivation of R_c

In an omni-directional scattering Rayleigh fading channel, the autocorrelation of the real part of the fading gain is [36]

$$R(\tau) = \sigma_g^2 J_0(2\pi f_D \tau). \tag{3.11}$$

Since calculation of the correlations for the data symbols is the same at all branches, we drop the subscripts $\{1,i\}$ and $\{2,i\}$ in (3.9) and (3.10). Then, combining (3.9) and (3.10) with (3.4a) and (3.11), we have

$$\begin{aligned} R_c = E[g^n_{lk} \hat{g}^n_{lk}] &= \sum_{k=-\lfloor \frac{K-1}{2} \rfloor}^{\lfloor \frac{K}{2} \rfloor} h^n_k E\left[g^n_{lk} \left(g^0_{lk} + \frac{n^0_{1,k} + n^0_{2,k}}{2} \right) \right] \\ &= \sum_{k=-\lfloor \frac{K-1}{2} \rfloor}^{\lfloor \frac{K}{2} \rfloor} \sigma_g^2 h^n_k J_0(2\pi f_D |kN - 2n| T_s). \end{aligned} \tag{3.12}$$

3.4.3 Derivation of $\sigma^2_{\hat{g}}$

From (3.9) and (3.10), the variance of $\hat{g}$ can be derived as

$$\begin{aligned} \sigma^2_{\hat{g}} &= \frac{1}{2} E[\hat{g}^n_k \hat{g}^{n*}_k] \\ &= \frac{1}{2} E\left[\sum_{k=-\lfloor \frac{K-1}{2} \rfloor}^{\lfloor \frac{K}{2} \rfloor} h^n_k \left(g^0_{1,i,k} + \frac{n^0_{1,i,k} + n^0_{2,i,k}}{2} \right) \sum_{k=-\lfloor \frac{K-1}{2} \rfloor}^{\lfloor \frac{K}{2} \rfloor} h^n_k \left(g^{0,*}_{1,i,k} + \frac{n^{0,*}_{1,i,k} + n^{0,*}_{2,i,k}}{2} \right) \right] \\ &= \sum_{k=-\lfloor \frac{K-1}{2} \rfloor}^{\lfloor \frac{K}{2} \rfloor} \sum_{m=-\lfloor \frac{K-1}{2} \rfloor}^{\lfloor \frac{K}{2} \rfloor} h^n_k h^n_m \sigma_g^2 J_0(2\pi f_D |k-m| N T_s) + \frac{\sigma_n^2}{2} \sum_{m=-\lfloor \frac{K-1}{2} \rfloor}^{\lfloor \frac{K}{2} \rfloor} (h^n_k)^2. \end{aligned} \tag{3.13}$$

3.4.4 Derivation of ρ

From (3.6), using (3.12) and (3.13), we have

$$\rho = \frac{R_c^2}{\sigma_g^2 \sigma_{\hat{g}}^2} = \frac{\left[\sum_{k=-\lfloor \frac{K-1}{2} \rfloor}^{\lfloor \frac{K}{2} \rfloor} h_k^n J_0(2\pi f_D |kN - 2n| T_s)\right]^2}{\sum_{k=-\lfloor \frac{K-1}{2} \rfloor}^{\lfloor \frac{K}{2} \rfloor} \sum_{m=-\lfloor \frac{K-1}{2} \rfloor}^{\lfloor \frac{K}{2} \rfloor} h_k^n h_m^n J_0(2\pi f_D |k-m| N T_s) + \frac{1}{\gamma_b} \sum_{m=-\lfloor \frac{K-1}{2} \rfloor}^{\lfloor \frac{K}{2} \rfloor} (h_k^n)^2} \quad (3.14)$$

Note that ρ is a function of the type of interpolator, the data symbol location, the Doppler shift, the data frame length and the symbol interval. When a sinc interpolator [37] is used and a Hamming window is applied, the interpolation coefficients are given by

$$h_k^n = \text{sinc}\left(\frac{2n}{N} - k\right)\left[0.54 - 0.46\cos\left(\frac{2\pi(2n - kN)}{KN - 1} + \frac{2\pi\lfloor \frac{KN}{2} \rfloor}{KN - 1}\right)\right]. \quad (3.15)$$

3.5 Conclusion

In this chapter, the space-time system was introduced. As one type of space-time system and the focus of this thesis, the Alamouti system was illustrated. Since the performance of the Alamouti system depends on the accuracy of channel estimation, the derivation of channel estimation errors for this system was given. In the next chapter, this channel estimation error will be quantified for Alamouti MIMO systems when receiver selection is applied. The effects of channel estimation errors on several receiver selection combining schemes will be investigated.

Chapter 4

Effects of Channel Estimation Errors on Receiver Selection Combining Schemes for Alamouti MIMO Systems

In this chapter, the BER of BPSK in Rayleigh fading using the Alamouti transmission scheme and receiver selection diversity in the presence of channel estimation error is studied. Closed-form expressions for the BER of LLR selection, SNR selection, SSC selection and MRC are derived in terms of the SNR and the cross-correlation coefficient of the channel gain and its corrupted estimate. The effects of channel estimation errors on each selection scheme are examined.

4.1 Introduction

In this chapter, we examine the effect of channel estimation error on the BER performance of a MIMO system using binary phase-shift keying modulation and receiver selection diversity in a slow flat Rayleigh fading channel. The Alamouti STBC [1] is used at the transmitter. The "best" of L Rx antennas is chosen according to some selection criterion. Since all selection combining schemes require some knowledge of the complex channel

gains for all the diversity branches and the complex channel gains have to be estimated at the receiver, channel estimation errors affect the performance of all practical selection combining schemes. Quantitative results for the effects of noisy channel estimation are derived.

Three different selection schemes are considered for Rx antenna selection. The first scheme is LLR selection, which was proposed in [30] for a 1 Tx antenna and L Rx antennas system. In LLR selection, full knowledge of all the complex diversity branch gains is needed and the branch providing the largest magnitude of LLR is chosen. This selection scheme was extended in [38] to include a 2 Tx antennas and N_R Rx antennas system using the Alamouti scheme. The BER for this scheme is given by an expression involving a single integral. However, perfect channel estimation is assumed in [38]. Here, we derive a closed-form BER expression for this LLR selection scheme, accounting for the presence of channel estimation errors.

Traditional selection combining is the second scheme considered in this paper. The selection of the best antenna is based on the largest SNR among the diversity branches at the detector input. Unlike LLR selection which requires full knowledge of the complex channel gains for all the diversity branches, SNR selection only requires ordering fading amplitudes on the diversity branches. In [38] and [10], the BER of SNR selection at the receiver side is evaluated. In this chapter, this result is extended to include the effects of channel estimation errors.

In order to implement all the former selection combining schemes, the receiver needs to monitor all the diversity branches to select the "best" branch. Furthermore, the receiver may switch frequently in order to use the best branches. It is desirable in some practical implementations to minimize switching in order to reduce switching transients. Therefore, selection combining is often implemented in the form of switched diversity [24], [25] in practical systems, in which rather than continuously picking the best branch, the receiver selects a particular branch until its SNR drops below a predetermined threshold. When this happens, the receiver switches to another branch. References [39] and [40] investigate a switched diversity system with 1 Tx antenna and N_R Rx antennas. A performance analysis

for this system without space-time coding was given in Rayleigh fading in [39] and in Nakagami fading in [40]. In this chapter, we analyze a transmission system with an Alamouti code at the Tx and switched diversity at the Rx. The average BER accounting for the effects of channel estimation error is derived and the optimal switching threshold that minimizes the BER for this switched diversity scheme is determined.

The remainder of this chapter is organized as follows. In Section 5.2, we consider a wireless system with 2 Tx antennas using the Alamouti scheme and L Rx antennas, and derive the BER for the three selection combining schemes with channel estimation errors considered. The analysis of MRC [2] is also recalled and the performances of these three selection schemes are compared to the optimal MRC scheme. In Section 5.3, numerical results are presented and the relative performances of the three selection schemes are discussed. Conclusions are drawn in Section 5.4.

4.2 Bit Error Rate Analysis

The system model used in this chapter is the same as in Chapter 3. By symmetry, the BER is the same for s_1 and s_2, so the following analysis will consider s_1 only. The results for s_i, $i = 1,2$ can be obtained by appropriately renaming the variables.

Using (3.1), (3.2), and (3.5), the combiner output $y_{1,i}$ can be written as

$$\begin{aligned} y_{1,i} = {} & b\left(|\hat{g}_{1,i}|^2 + |\hat{g}_{2,i}|^2\right) s_1 + \left(\hat{g}_{1,i}^* d_{1,i} + \hat{g}_{2,i} d_{2,i}^*\right) s_1 \\ & + \left(\hat{g}_{1,i}^* d_{2,i} - \hat{g}_{2,i} d_{1,i}^*\right) s_2 + \hat{g}_{1,i}^* n_{1,i} + \hat{g}_{2,i} n_{2,i}^*. \end{aligned} \tag{4.1}$$

Since $s_2 = +s_1$ or $-s_1$, each with probability $1/2$, we can calculate the BER as $P_b = 1/2(P_{b,s_2=s_1} + P_{b,s_2=-s_1}) = P_{b,s_2=s_1} = P_{b,s_2=s_1=1}$, where the last two equations follow from symmetry. For the case $s_2 = s_1 = 1$, we can write the decision variable as

$$\begin{aligned} Re(y_{1,i}) = {} & b\left(|\hat{g}_{1,i}|^2 + |\hat{g}_{2,i}|^2\right) + Re\left[\hat{g}_{1,i}^*(d_{1,i} + d_{2,i})\right. \\ & \left. + \hat{g}_{2,i}(d_{2,i} - d_{1,i})^*\right] + Re(\hat{g}_{1,i}^* n_{1,i}) + Re(\hat{g}_{2,i} n_{2,i}^*). \end{aligned} \tag{4.2}$$

Normalizing the expression in (4.2) by dividing both sides of the equation with $\frac{1}{2b\sigma_{\hat{g}}^2}$, we have

$$Re(y'_{1,i}) = \frac{1}{2\sigma_{\hat{g}}^2}\left(|\hat{g}_{1,i}|^2 + |\hat{g}_{2,i}|^2\right) + \frac{1}{2b\sigma_{\hat{g}}^2} \times Re\left[\hat{g}_{1,i}^*(d_{1,i} + d_{2,i} + n_{1,i}) + \hat{g}_{2,i}(d_{2,i} - d_{1,i} + n_{2,i})^*\right]. \tag{4.3}$$

Conditioning on $|\hat{g}_{1,i}|^2$ and $|\hat{g}_{2,i}|^2$, it can be shown that $Re\left[\hat{g}_{1,i}^*(d_{1,i}+d_{2,i})\right]$, $Re\left[\hat{g}_{2,i}^*(d_{2,i}-d_{1,i})\right]$, $Re(\hat{g}_{1,i}^* n_{1,i})$ and $Re(\hat{g}_{2,i} n_{2,i}^*)$ are independent, zero-mean Gaussian random variables with variance $2|\hat{g}_{1,i}|^2\sigma_d^2$, $2|\hat{g}_{2,i}|^2\sigma_d^2$, $|\hat{g}_{1,i}|^2\sigma_n^2$ and $|\hat{g}_{2,i}|^2\sigma_n^2$, respectively. Therefore, $Re(y'_{1,i})$, conditioned on $|\hat{g}_{1,i}|^2$ and $|\hat{g}_{2,i}|^2$, is a Gaussian random variable as well. It has mean $\frac{1}{2\sigma_{\hat{g}}^2}\left(|\hat{g}_{1,i}|^2 + |\hat{g}_{2,i}|^2\right)$ and variance $\frac{2\sigma_d^2+\sigma_n^2}{4b^2\sigma_{\hat{g}}^4}\left(|\hat{g}_{1,i}|^2 + |\hat{g}_{2,i}|^2\right)$. Let $\alpha_i = \frac{|\hat{g}_{1,i}|^2+|\hat{g}_{2,i}|^2}{2\sigma_{\hat{g}}^2}$; conditioned on α_i, the new decision variable $Re(y'_{1,i})$ has mean α_i and variance $\frac{(2\sigma_d^2+\sigma_n^2)}{2b^2\sigma_{\hat{g}}^2}\alpha_i$. Using (3.6) and $\sigma_d^2 = (1-\rho)\sigma_g^2$ [35], this variance is simplified to $\frac{(1-\rho)\bar{\gamma}_b+1}{\rho\bar{\gamma}_b}\alpha_i$. Define the effective SNR

$$\bar{\gamma}_c = \frac{\rho\bar{\gamma}_b}{(1-\rho)\bar{\gamma}_b + 1}. \tag{4.4}$$

Then the variance is $\frac{\alpha}{\bar{\gamma}_c}$.

Since $\hat{g}_{1,i}$ and $\hat{g}_{2,i}$ are independent, zero-mean complex Gaussian random variables, α_i has a chi-square distribution with 4 degrees of freedom and its pdf is given by [2]

$$f_A(\alpha_i) = \alpha_i \exp\left(-\alpha_i\right). \tag{4.5}$$

4.2.1 LLR selection combining

The LLR Rx selection system model is described in [38] and shown in Fig. 4.1. The LLR Λ_i for data s_1, given $\hat{g}_{j,i}$ and $y_{1,i}$ is [38]

$$\Lambda_i = \ln\frac{P\left(s_1 = +1|\hat{g}_{j,i}, y_{1,i}\right)}{P\left(s_1 = -1|\hat{g}_{j,i}, y_{1,i}\right)} = \frac{4}{N_0}\mathrm{Re}(y_{1,i}) = \frac{8b\sigma_{\hat{g}}^2}{N_0}\mathrm{Re}(y'_{1,i}). \tag{4.6}$$

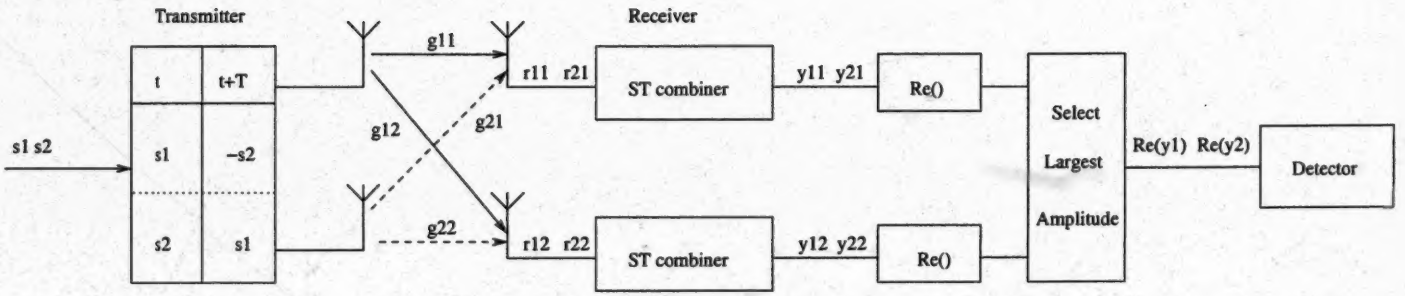

Fig. 4.1. The LLR receiver selection system model.

Thus, with the Alamouti scheme, the LLR Rx selection combining is equivalent to selecting the branch providing the largest amplitude of $\mathrm{Re}(y'_{1,i})$.

Conditioning the expression for $\mathrm{Re}(y'_{1,i})$ in (4.3) on $\hat{g}_{1,i}$ and $\hat{g}_{2,i}$, yields

$$\begin{aligned} P_b &= \sum_{i=1}^{L} \Pr(\mathrm{Re}(y'_{1,i}) < 0, i\text{th branch selected}) \\ &= L \Pr\left(\mathrm{Re}(y'_{1,1}) < 0, 1\text{th branch selected}\right) \\ &= L \Pr\left(\mathrm{Re}(y'_{1,1}) < 0, \left|\mathrm{Re}(y'_{1,1})\right| > \left|\mathrm{Re}(y'_{1,i})\right|_{\forall i, i\neq 1}\right). \end{aligned} \tag{4.7}$$

Let $r_i = \mathrm{Re}(y'_{1,i})$ and $r_1 = -\mathrm{Re}(y'_{1,1})$, then

$$P_b = L \int_0^{\infty} \left[\Pr\left(-r_1 < r_i < r_1 \middle| r_1\right)\right]^{L-1} f_R(r_1) dr_1 \tag{4.8}$$

where $f_R(r_1)$ is the pdf of r_1.

Since $r_1 = -\mathrm{Re}(y'_{1,1})$, $f_R(r_1)$ is equal to $f_{r_i}(-r_1)$, where $f_{r_i}(x)$ is the pdf of r_i. From (4.3), one has that $\mathrm{Re}(y'_{1,i})_{\forall i, i\neq 1}$ is Gaussian distributed with mean α_i and variance $\frac{\alpha_i}{\bar{\gamma}_c}$, when conditioned on $\alpha_i = \frac{|\hat{g}_{1,i}|^2 + |\hat{g}_{2,i}|^2}{2\sigma_{\hat{g}}^2}$. Averaging over α_i, the pdf of r_i is given by

$$\begin{aligned} f_{r_i}(x) &= \int_0^{\infty} f_{r_i}(x|\alpha_i) f_A(\alpha_i) d\alpha_i \\ &= \int_0^{\infty} \sqrt{\frac{\bar{\gamma}_c}{2\pi\alpha_i}} \exp\left[-\frac{\bar{\gamma}_c (x-\alpha_i)^2}{2\alpha_i}\right] \alpha_i \exp\left(-\alpha_i\right) d\alpha_i. \end{aligned} \tag{4.9}$$

Changing the variable of integration to $z = \sqrt{\alpha_i}$, and using the result from [41, eq. (3.472)], (4.9) can be simplified as

$$\begin{aligned} f_{r_i}(x) &= A\left(1 + B|x|\right) \exp\left(-B|x| + Cx\right) \\ A &= \frac{\sqrt{\bar{\gamma}_c(\bar{\gamma}_c + 2)}}{(\bar{\gamma}_c + 2)^2} \qquad B = \sqrt{\bar{\gamma}_c(\bar{\gamma}_c + 2)} \\ C &= \bar{\gamma}_c. \end{aligned} \tag{4.10}$$

Then, for the ith branch

$$\begin{aligned} \Pr\left(-r_1 < r_i < r_1 \middle| r_1\right) &= \int_{-r_1}^{r_1} f_{r_i}(x) dx \\ &= k_7 + (k_1 - k_2 r_1) \exp\left(-k_3 r_1\right) - (k_4 + k_5 r_1) \exp\left(-k_6 r_1\right) \end{aligned} \tag{4.11}$$

$$k_1 = \frac{AC-2AB}{(C-B)^2} \qquad k_2 = \frac{AB}{B-C}$$
$$k_3 = B-C \qquad k_4 = \frac{2AB+AC}{(B+C)^2}$$
$$k_5 = \frac{AB}{B+C} \qquad k_6 = B+C$$
$$k_7 = \frac{4AB^3}{(B^2-C^2)^2}.$$

Combining (4.8), (4.10) and (4.11), the final expression for the BER is obtained as

$$\begin{aligned} P_b &= L\int_0^\infty \left[k_7 + (k_1 - k_2 r_1)\exp(-k_3 r_1)\right. \\ &\quad \left. -(k_4 + k_5 r_1)\exp(-k_6 r_1)\right]^{L-1} \\ &\quad \times A(1+Br_1)\exp(-Br_1 - Cr_1)\,dr_1 \\ &= L\sum_{n=0}^{L-1}\sum_{m=0}^{L-1-n}\sum_{p=0}^{n}\sum_{q=0}^{m}\sum_{i=0}^{1}\binom{L-1}{n\ m}\binom{n}{p}\binom{m}{q} \\ &\quad \times AB^i k_1^{n-p} k_2^p k_4^{m-q} k_5^q k_7^{L-1-n-m} \frac{(-1)^{m+p}(p+q+i)!}{(k_3 n + k_6 m + B + C)^{p+q+i+1}}. \end{aligned} \tag{4.12}$$

A simpler sub-optimum selection combining rule was also proposed by Kim and Kim in [30]. The system model is plotted in Fig. 4.2. Instead of the amplitude of $\mathrm{Re}(y_{1,i})$, $|(y_{1,i})|$ is used for this envelope-LLR selection combining. The system model is shown in Fig. 4.2. Simulation results for the BER of this envelope-LLR selection scheme will be given together with results for the other selection combining schemes in Section 4.3.

4.2.2 *SNR* Selection Combining

The Rx selection combining scheme model is illustrated in Fig. 4.3. It is same as the model in [38] and [10]. In SNR selection combining, the Rx antenna with the largest SNR will be chosen for space-time decoding. From (4.2), the SNR, given the ith Rx antenna selected, is $\frac{b^2(|\hat{g}_{1,i}|^2+|\hat{g}_{2,i}|^2)}{2(2\sigma_d^2+\sigma_n^2)} = \frac{\bar{\gamma}_c \alpha_i}{2}$. Therefore, the antenna providing the largest SNR is the one providing the largest α_i. Let $A_{max} = \max[\alpha_i]$. Then, the expression of the BER can be

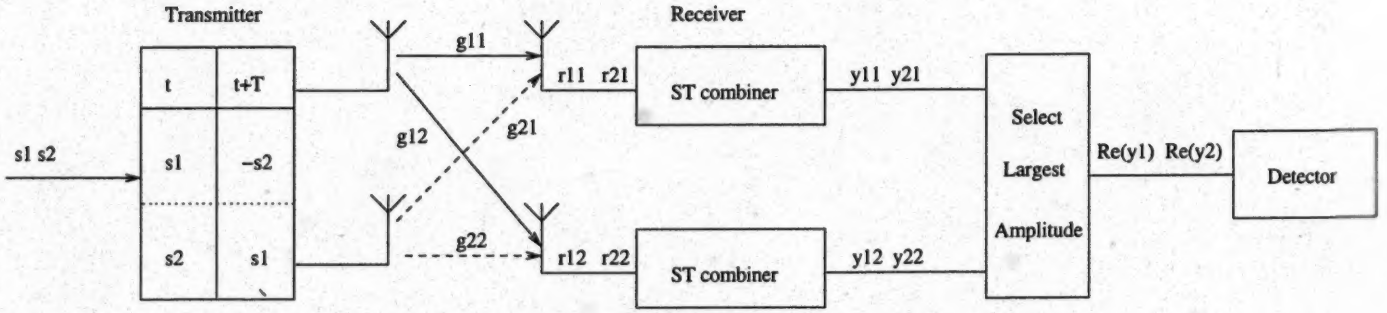

Fig. 4.2. The envelope-LLR receiver selection system model.

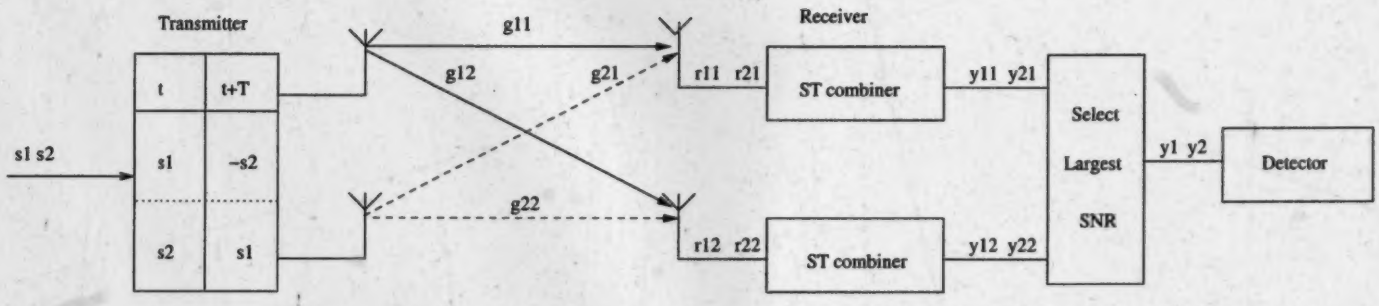

Fig. 4.3. The SNR receiver selection system model.

rewritten as [38]

$$P_b = \int_0^\infty \Pr\left(Re(y_{1,i}) \le 0 \middle| A_{max}\right) f_{A_{max}}(\alpha) d\alpha \tag{4.13a}$$
$$= \int_0^\infty \mathrm{Q}\left(\sqrt{\bar{\gamma}_c \alpha}\right) f_{A_{max}}(\alpha) d\alpha$$

where the pdf of A_{max} is [42]

$$f_{A_{max}}(\alpha) = L\left[\int_0^\alpha f_A(\alpha_i) d\alpha_i\right]^{L-1} f_A(\alpha) \tag{4.13b}$$
$$= L[1-(1+\alpha)\exp(-\alpha)]^{L-1} f_A(\alpha)$$

and $f_A(\alpha)$ is given in (4.5).

Expanding $\left[\int_0^\alpha f_A(\alpha) d\alpha\right]^{L-1}$ in (4.13a) using the binomial theorem gives

$$P_b = L \sum_{i=0}^{L-1} \sum_{j=0}^{i} \binom{L-1}{i} \binom{i}{j} (-1)^i \tag{4.14}$$
$$\times \int_0^\infty \mathrm{Q}\left(\sqrt{\bar{\gamma}_c \alpha}\right) \alpha^{j+1} \exp[-(i+1)\alpha] d\alpha.$$

Integrating (4.14) term-by-term, the final expression for the BER is derived as

$$P_b = L \sum_{i=0}^{L-1} \sum_{j=0}^{i} \sum_{m=0}^{j+1} (-1)^i \binom{L-1}{i} \binom{i}{j} \tag{4.15a}$$
$$\times \frac{(j+1+m)!}{m!(1+i)^{j+2}} \left(\frac{1-\mu_1}{2}\right)^{j+2} \left(\frac{1+\mu_1}{2}\right)^m$$

$$\mu_1 = \sqrt{\frac{\bar{\gamma}_c}{\bar{\gamma}_c + 2i + 2}}. \tag{4.15b}$$

4.2.3 Switch-and-Stay Selection

The system model is shown in Fig. 4.4. In Rx SSC, with channel estimation error, the BER is related to the instantaneous effective SNR of the selected ith branch γ_c in (4.2), where $\gamma_c = \frac{k^2\left(|\hat{g}_{1,i}|^2 + |\hat{g}_{2,i}|^2\right)}{2(2\sigma_d^2 + \sigma_n^2)} = \frac{\bar{\gamma}_c \alpha_i}{2}$. Conditioning on the pdf of γ_c, the BER is $\mathrm{Q}(\sqrt{2\gamma_c})$.

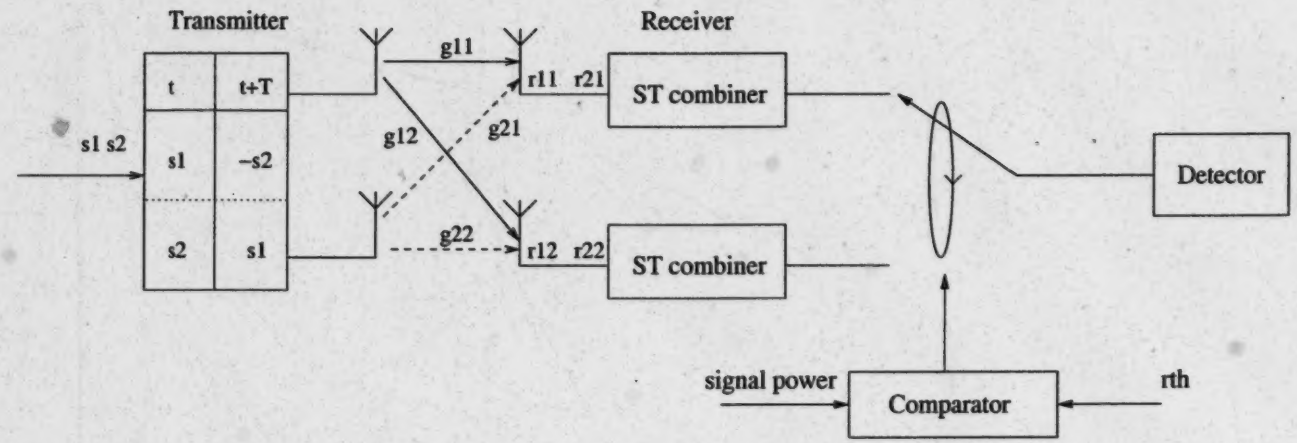

Fig. 4.4. The SSC receiver selection system model.

Following [40], the cumulative distribution function (cdf) of γ_c can be written as

$$F_X(\gamma_c) = \begin{cases} \Pr(\gamma_{c,1} \le \gamma_c)\Pr(\gamma_{c,2} \le \gamma_c), & \text{if } \gamma_c < \gamma_{th} \\ \Pr(\gamma_{th} \le \gamma_{c,1} \le \gamma_c) & \\ +\Pr(\gamma_{c,1} \le \gamma_c)\Pr(\gamma_{c,2} \le \gamma_c), & \text{if } \gamma_c \ge \gamma_{th} \end{cases} \tag{4.16}$$

where $\gamma_{c,1}$ and $\gamma_{c,2}$ are the instantaneous SNR on the 1st and 2nd Rx branches, respectively. Since $\gamma_c = \frac{\bar{\gamma}_c \alpha_i}{2}$, from (4.5), both $\gamma_{c,1}$ and $\gamma_{c,2}$ have a chi-squared distribution given by

$$f(\gamma_{c,i}) = \frac{4\gamma_{c,i}}{\bar{\gamma}_c^2} \exp\left(-\frac{2\gamma_{c,i}}{\bar{\gamma}_c}\right), \quad i = 1,2. \tag{4.17}$$

The pdf is obtained by differentiating the cdf in (4.16) with respect to γ_c

$$f(\gamma_c) = \begin{cases} (1 - e^{-\frac{\gamma_{th}}{\bar{\gamma}_c}})\frac{1}{\bar{\gamma}_c} e^{-\frac{\gamma_c}{\bar{\gamma}_c}} & \gamma_c < \gamma_{th} \\ (2 - e^{-\frac{\gamma_{th}}{\bar{\gamma}_c}})\frac{1}{\bar{\gamma}_c} e^{-\frac{\gamma_c}{\bar{\gamma}_c}} & \gamma_c \ge \gamma_{th}. \end{cases} \tag{4.18}$$

Then, the BER is

$$\begin{aligned} P_b &= \int_0^\infty Q\left(\sqrt{2\gamma_c}\right) f(\gamma_c) d\gamma_c \qquad (4.19) \\ &= K_4 \int_0^\infty Q(\sqrt{2\gamma_c}) \frac{4\gamma_c}{\bar{\gamma}_c^2} \exp\left(-\frac{2\gamma_c}{\bar{\gamma}_c}\right) d\gamma_c \\ &+ \int_{\gamma_{th}}^\infty Q(\sqrt{2\gamma_c}) \frac{4\gamma_c}{\bar{\gamma}_c^2} \exp\left(-\frac{2\gamma_c}{\bar{\gamma}_c}\right) d\gamma_c \\ &= K_1 - K_2 Q\left[K_3(\bar{\gamma}_c + 2)\right] - \exp\left(-\frac{2\gamma_{th}}{\bar{\gamma}_c}\right) \times \\ &\left\{(K_3 + 1)\left[K_1 - Q(\sqrt{2\gamma_{th}})\right] + \frac{\sqrt{\gamma_{th}}}{\sqrt{\pi}(\bar{\gamma}_c + 2)} \exp(-\gamma_{th})\right\} \end{aligned}$$

$$\begin{aligned} K_1 &= \frac{\sqrt{(\bar{\gamma}_c + 2)^3} - \bar{\gamma}_c\sqrt{\bar{\gamma}_c} - 3\sqrt{\bar{\gamma}_c}}{2\sqrt{(\bar{\gamma}_c + 2)^3}} \\ K_2 &= \frac{\bar{\gamma}_c + 3}{\bar{\gamma}_c + 2}\sqrt{\frac{\bar{\gamma}_c}{\bar{\gamma}_c + 2}} \\ K_3 &= \frac{2\gamma_{th}}{\bar{\gamma}_c} \\ K_4 &= 1 - \left(\frac{2\gamma_{th}}{\bar{\gamma}_c} + 1\right) \exp\left(-\frac{2\gamma_{th}}{\bar{\gamma}_c}\right). \end{aligned}$$

Note that the BER depends on the value of the switching threshold, γ_{th}. The optimal value, γ_{th}^*, is a solution of the equation $\frac{\partial P_e}{\partial \gamma_{th}}\Big|_{\gamma_{th}=\gamma_{th}^*} = 0$. Differentiating (4.19) with respect to γ_{th}, we get

$$\gamma_{th}^* = \frac{1}{2}\left[Q^{-1}(\alpha)\right]^2 \tag{4.20a}$$

$$\alpha = \frac{1}{2} - \frac{\bar{\gamma}_c\sqrt{\bar{\gamma}_c}}{2\sqrt{(\bar{\gamma}_c+2)^3}} - \frac{3\sqrt{\bar{\gamma}_c}}{2\sqrt{(\bar{\gamma}_c+2)^3}} \tag{4.20b}$$

where $Q^{-1}(\cdot)$ denotes the inverse Gaussian Q-function, and $\bar{\gamma}_c$ is the effective SNR (4.4).

4.2.4 MRC Diversity

In MRC, all the combiner outputs are weighted and summed to form the decision variable as illustrated in Fig. 4.5. From (4.3), the combiner output is

$$\begin{aligned}\mathrm{Re}\left[\sum_{i=1}^{L} y'_{1,i}\right] &= \frac{1}{2\sigma_{\hat{g}}^2}\sum_{i=1}^{L}\left(|\hat{g}_{1i}|^2+|\hat{g}_{2i}|^2\right) + \frac{1}{2k\sigma_{\hat{g}}^2}\times \\ &\mathrm{Re}\sum_{i=1}^{L}\left[\hat{g}_{1,i}^*(d_{1,i}+d_{2,i}+n_{1,i}) + \hat{g}_{2,i}(d_{2,i}-d_{1,i}+n_{2,i})^*\right].\end{aligned} \tag{4.21}$$

Conditioned on $y = \frac{\Sigma_{i=1}^{L}\left(|\hat{g}_{1i}|^2+|\hat{g}_{2i}|^2\right)}{2\sigma_{\hat{g}}^2}$, this decision variable is a Gaussian random variable with mean y and variance $\frac{y}{\bar{\gamma}_c}$. The pdf of y is chi-square distributed with $4L$ degrees of freedom [2]

$$\frac{1}{(2L-1)!}y^{2L-1}\exp(-y). \tag{4.22}$$

Following [2], the BER for MRC with Alamouti coding is obtained as

$$\begin{aligned}P_b &= \int_0^\infty \mathrm{Q}\left(\sqrt{\bar{\gamma}_c y}\right)\frac{1}{(2L-1)!}y^{2L-1}\exp(-y)dy \\ &= \left[\frac{1}{2}(1-\mu_2)\right]^{2L}\sum_{k=0}^{2L-1}\binom{2L-l+k}{k}\left[\frac{1}{2}(1+\mu_2)\right]^k\end{aligned} \tag{4.23a}$$

$$\mu_2 = \sqrt{\frac{\bar{\gamma}_c}{\bar{\gamma}_c+2}}. \tag{4.23b}$$

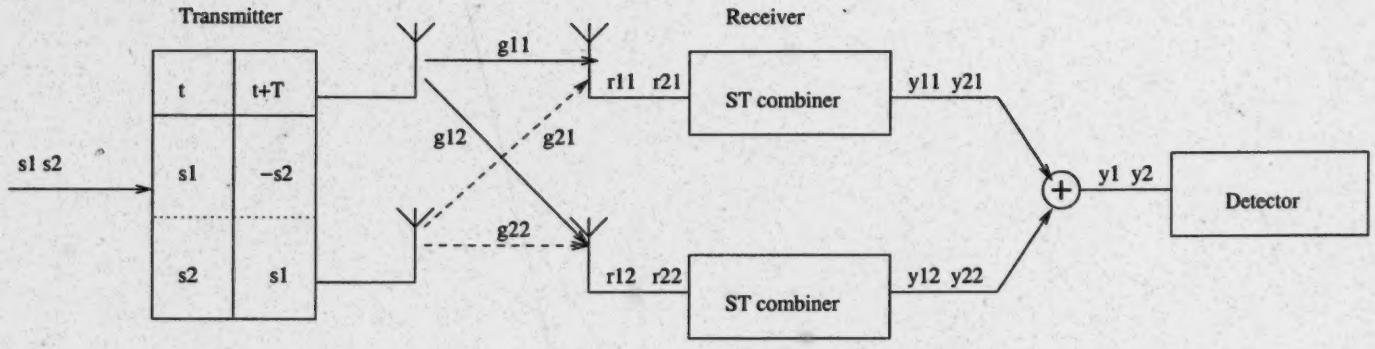

Fig. 4.5. The MRC receiver system model.

4.3 Numerical Results and Discussion

In this section, all the figures are generated from Mento Carlo simulation by using Matlab. The simulation results for LLR selection, SNR selection, SSC selection, and MRC verify the closed-form BER expressions in (4.12), (4.15), (4.19), and (4.23), respectively. Sufficient simulation run times are executed to obtain smooth BER curves. Here we use the number of simulation run times equal to $\frac{10^3}{P_T}$, where P_T is the target error probability.

The BER results are functions of $\bar{\gamma}_c$, which is in turn a function of ρ and $\bar{\gamma}_b$. Figs. 4.6–4.8 show plots of the average BER versus SNR per bit, $\bar{\gamma}_b$, for the different selection diversity schemes in a flat Rayleigh fading channel with perfect channel estimation, cross-correlation 0.9, and cross-correlation 0.75, respectively. The *envelope*-selection is evaluated by computer simulation. As expected, these results show that, in all cases, the BER increases with increasing fading estimation error (decreasing value of ρ).

It is observed in Figs. 4.6–4.8 that the performances of LLR selection and MRC are the same for dual diversity. The performances are, indeed, identical because, for MRC the sign of the combiner output $Re(y_{1,1}) + Re(y_{1,2})$ is determined by the maximum of $Re(y_{1,i})$, which coincides with the LLR selection rule. The envelope-LLR selection scheme, which does require channel estimation of all the channels, performs better than the SNR selection schemes but not as well as the LLR and MRC designs. The SSC selection offers the poorest performance, in exchange for its simplicity, as expected.

Figs. 4.9–4.11 show the average BER as a function of SNR per bit for the various selection schemes used in 4-fold diversity with perfect channel estimation, $\rho = 0.9$, and $\rho = 0.75$, respectively. There are a number of interesting observations. First, MRC and LLR are not the same, and MRC outperforms LLR, as expected. Second, the LLR selection outperforms envelope-LLR selection. Third, the envelope-LLR selection outperforms the SNR selection.

Figs. 4.6 – 4.11 show the average BER vs. SNR for specific, constant values of ρ for $L = 2$ and $L = 4$, respectively. These results show clearly the performance differences between the selection schemes. They are also representative of a situation where the receiver

electronics has reached a limit and cannot provide a better estimate of the channel gain. On the other hand, many practical estimators will show a dependence on SNR, i.e. give better estimates as the SNR increases. In these cases, a larger SNR value leads to a better channel estimate, which means a higher value of ρ. To show this effect on BER, we consider PSAM as an example. We assume that a sinc interpolator with a Hamming window is used to interpolate fading estimates, with a frame size of 14, and normalized Doppler shift of 0.03. Fig. 4.12 and Fig. 4.13 show the average BER versus SNR from 0 dB to 10 dB with $L = 2$ and $L = 4$, respectively. Since ρ is also a function of the symbol location, that is, with the same SNR value, in the same frame, data symbols located at different places will experience different ρ values, we give the BER of the 3rd symbol cluster in a frame as an example. Computed from (3.14), the value of ρ for this PSAM system varies from 0.513 to 0.913 as the SNR varies from 0 dB to 10 dB. Similar to the results in Figs. 4.6–4.11 , in Figs. 4.12 and 4.13, MRC and LLR selection still have the best performance for $L = 2$, then envelope-LLR selection outperforms SNR selection. The simplest selection scheme, SSC selection, has the worst BER performance. For $L = 4$, MRC outperforms LLR selection.

4.4 Conclusion

In this chapter, analytical BER results were derived for LLR selection, SNR selection, SSC and MRC with channel estimation errors using Alamouti transmission systems. The effects of channel estimation errors on each selection scheme were examined. In the next chapter, two new selection combining diversity schemes will be proposed and the effects of channel estimation errors on these two schemes will be investigated.

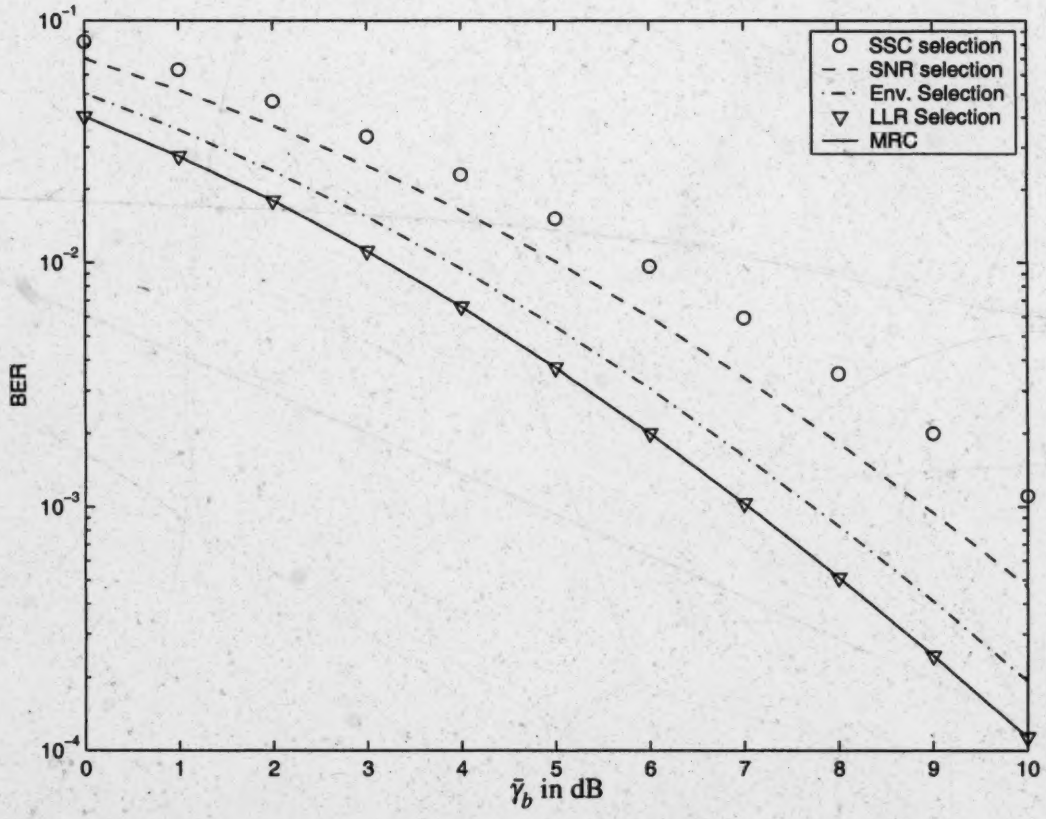

Fig. 4.6. The BER versus SNR for the 2 TX and 2 Rx, space-time block code with $\rho = 1$.

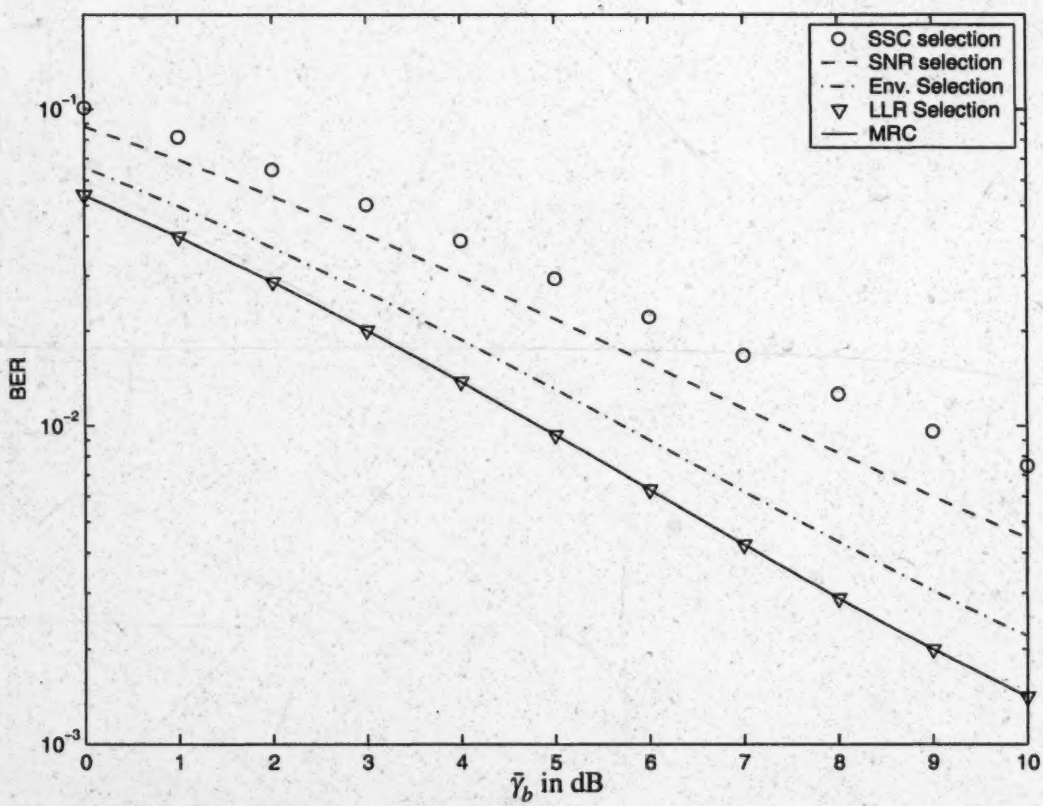

Fig. 4.7. The BER versus SNR for the 2 TX and 2 Rx, space-time block code with $\rho = 0.9$.

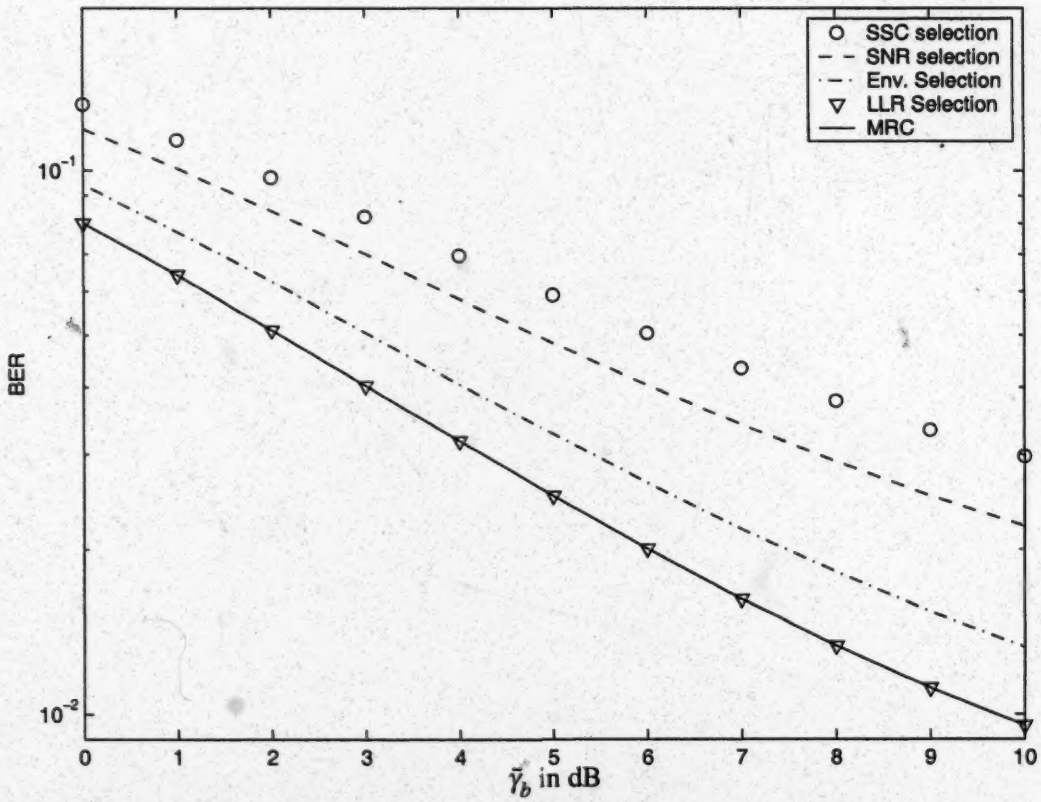

Fig. 4.8. The BER versus SNR for the 2 TX and 2 Rx, space-time block code with $\rho = 0.75$.

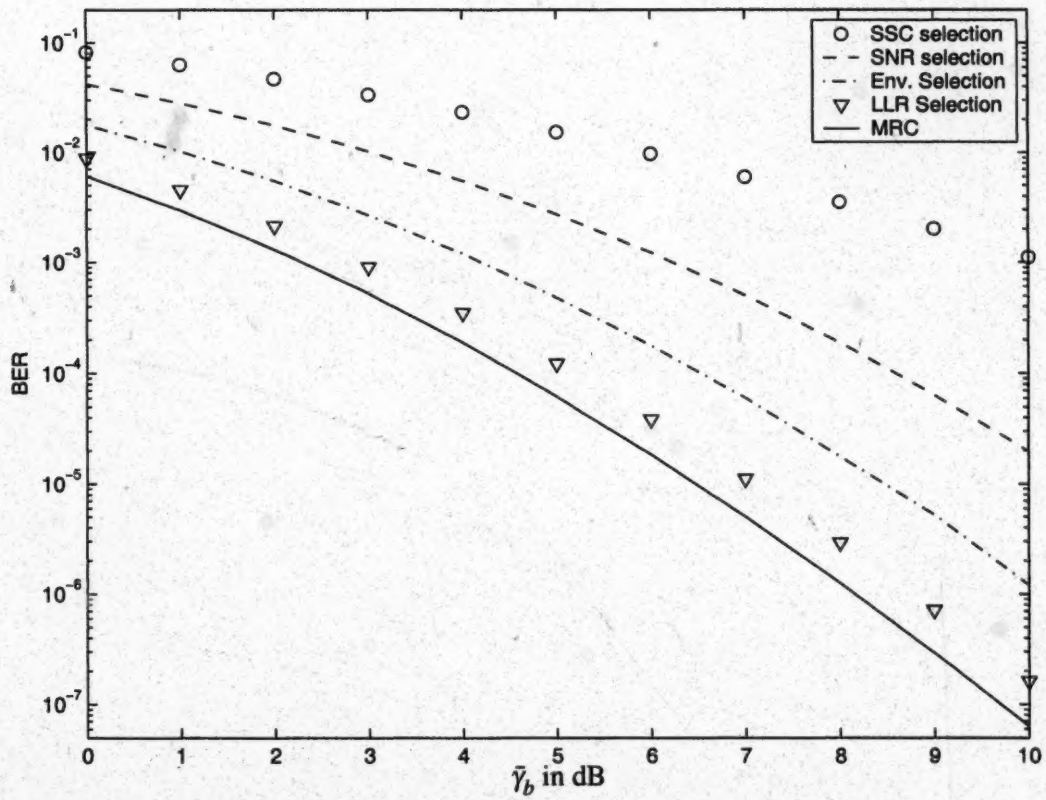

Fig. 4.9. The BER versus SNR for the 2 TX and 4 Rx, space-time block code with $\rho = 1$.

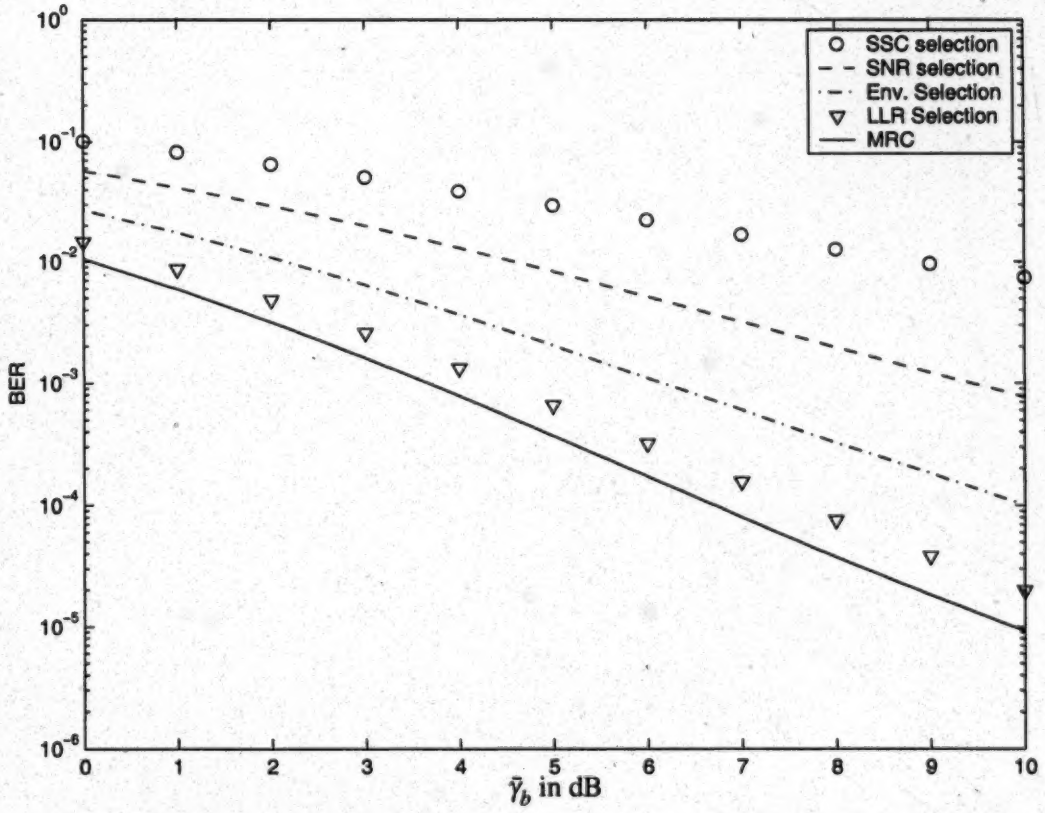

Fig. 4.10. The BER versus SNR for the 2 TX and 4 Rx, space-time block code with $\rho = 0.9$.

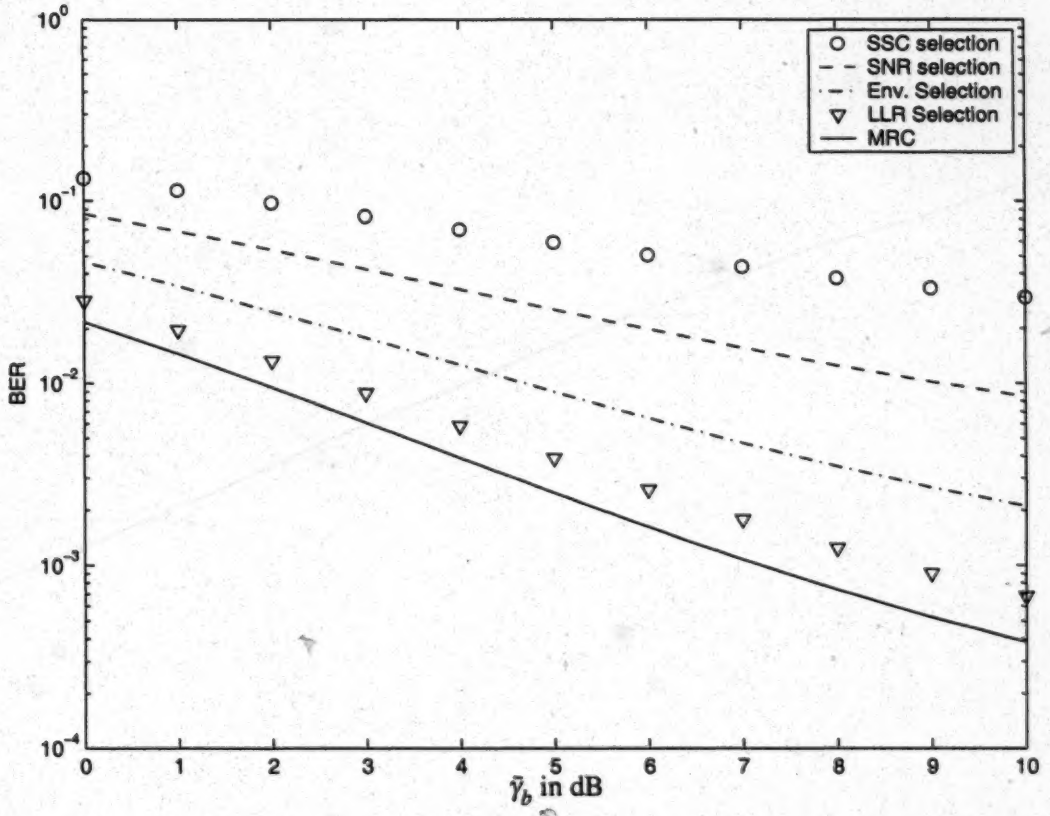

Fig. 4.11. The BER versus SNR for the 2 TX and 4 Rx, space-time block code with $\rho = 0.75$.

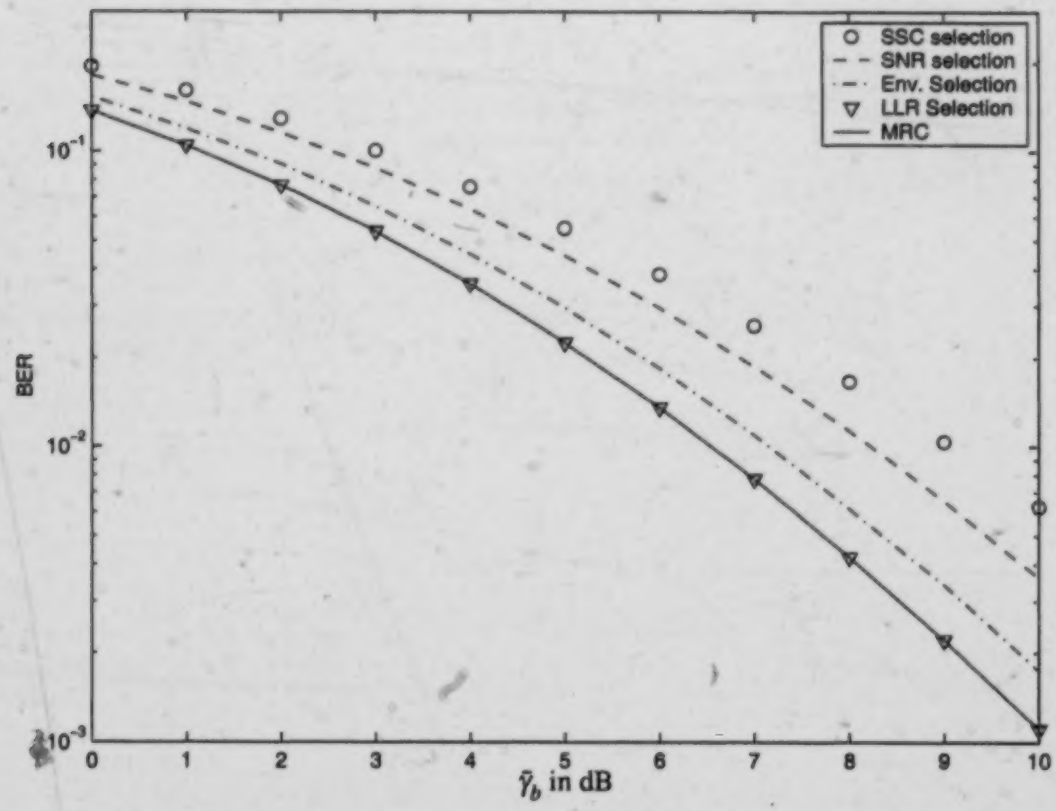

Fig. 4.12. The PSAM BER versus SNR for the 2 Tx and 2 Rx, Alamouti space-time block code with Hamming windowing applied to a sinc interpolator for $K = 30$, $N = 14$ and $f_D T_s = 0.03$ with symbol location at $n = 3$.

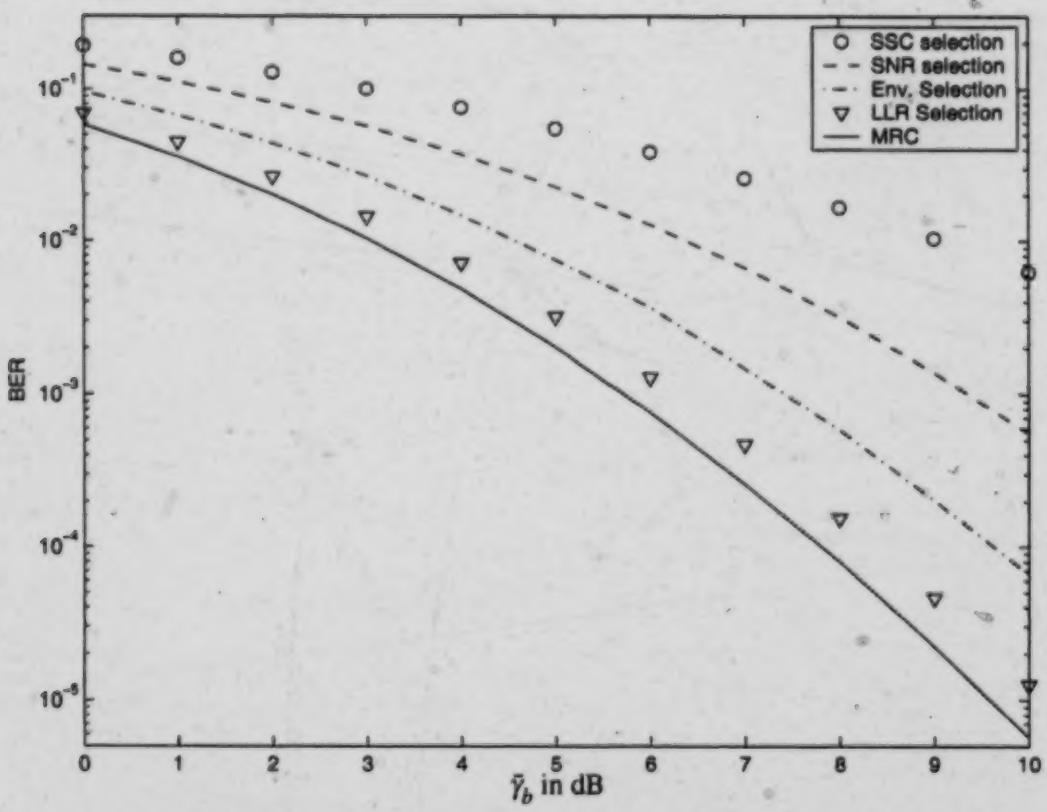

Fig. 4.13. The PSAM BER versus SNR for the 2 Tx and 4 Rx, Alamouti space-time block code with Hamming windowing applied to a sinc interpolator for $K = 30$, $N = 14$ and $f_D T_s = 0.03$ with symbol location at $n = 3$.

Chapter 5

Receiver Selection Diversity Schemes without Channel Estimation for Alamouti MIMO Systems

In this chapter, two new receiver selection schemes, space-time square-law (STSL) selection diversity and space-time magnitude (STM) selection diversity, are proposed for a MIMO system using the Alamouti STBC at the transmitter in a slow, flat Rayleigh fading channel. The BER of BPSK in Rayleigh fading using these two selection schemes is studied and compared to that of previous selection schemes. The effects of channel estimation errors on each selection scheme are examined in detail. Both proposed schemes are indicated in this chapter with much simpler hardware implementation but offer comparable performance with SNR selection method.

5.1 Introduction

Previous selection schemes include SNR selection, LLR selection, and SSC selection. SNR selection requires knowledge of the fading channel amplitudes on all receiver antennas in order to select the diversity branches with the largest values of SNR among the diversity

branches at the detector input. In LLR selection, full knowledge of all the complex diversity branch gains is needed and the branch providing the largest magnitude of LLR is chosen. As a result, it provides better BER performance than that of SNR selection. The SSC selection is a much simpler scheme, compared to the two previous selection schemes, as it does not need to monitor all the diversity branches and only switches when the SNR of the current chosen branch drops below a predetermined threshold. However, the knowledge of the fading channel amplitude of the selected branch is still needed.

Since all the selection schemes discussed above require channel knowledge, we propose a new selection scheme, which we will refer to as STSL selection. The STSL selection scheme does not require knowledge of the channel gains to make the Rx antenna selection. Furthermore, branch selection is done before the space-time decoding so that channel estimation for the space-time decoding is only performed for the branch selected, achieving a significant complexity reduction. Compared to the two former schemes, this new scheme is much simpler to implement. Significantly, it is shown in the sequel that it provides essentially the same performance as the SNR selection scheme.

The proposed STSL selection combining requires squaring the amplitudes of the received bit signals before making the selection. In order to further simplify the hardware implementation, we propose another scheme which only needs the amplitudes of the received bit signals. Similar to STSL selection, this scheme, called STM selection, does not require channel estimation. The simulation results in the following section show that STM selection has only slightly poorer BER performance than STSL and SNR selection.

The remainder of this chapter is organized as follows. In Section 5.2, we consider a wireless system with 2 Tx antennas using the Alamouti scheme and L Rx antennas, and propose the new selection schemes. In Section 5.3, numerical results are presented and the performances of all the selection schemes are discussed. Conclusions are drawn in Section 5.4.

5.2 New Selection Combining Methods

Both *LLR*-based and *SNR*-based selection combining schemes require knowledge of all the receiver branch fading gains in order to decide which branch to choose. This increases the receiver complexity. Here, we propose two new selection diversity schemes that do not require channel estimation for the selection.

5.2.1 Method 1: Space-Time Square-Law Selection

Here, we propose a new selection diversity scheme that selects the branch providing the largest sum of the squared amplitudes of the two received bit signals, i.e. $|r_{1,i}|^2+|r_{2,i}|^2$ (see Fig. 5.1). This scheme is similar to square-law combining, although square-law combining is used for noncoherent modulation and we deal with coherent modulation here. To the best of the authors' knowledge, this selection combining diversity scheme as used in space-time coding here with coherent modulation is novel. We will call it space-time square-law selection.

The advantage of this selection scheme is that it does selection before ST combining and it does not require channel estimation to perform the selection. Thus, we only need one ST combiner and one channel estimator for all the L receiver branches. Compared to all the pre-existing selection schemes, which need L ST combiners and L channel estimators for all L receiver branches, this is a big hardware saving. Hence, the receiver implementation is simpler than other selection schemes. Moreover, this new scheme provides the same performance with *SNR*-based selection, as is shown in Section 5.3. The reason is explained as follows.

Observe that

$$\begin{aligned} 2|r_{1,i}|^2+2|r_{2,i}|^2 &= |r_{1,i}+r_{2,i}|^2+|r_{1,i}-r_{2,i}|^2 \qquad (5.1a)\\ &= \left|g_{1,i}(s_1-s_2)+g_{2,i}(s_1+s_2)+n_{1,i}+n_{2,i}\right|^2 \\ &+ \left|g_{1,i}(s_1+s_2)+g_{2,i}(s_2-s_1)+n_{1,i}-n_{2,i}\right|^2 \end{aligned}$$

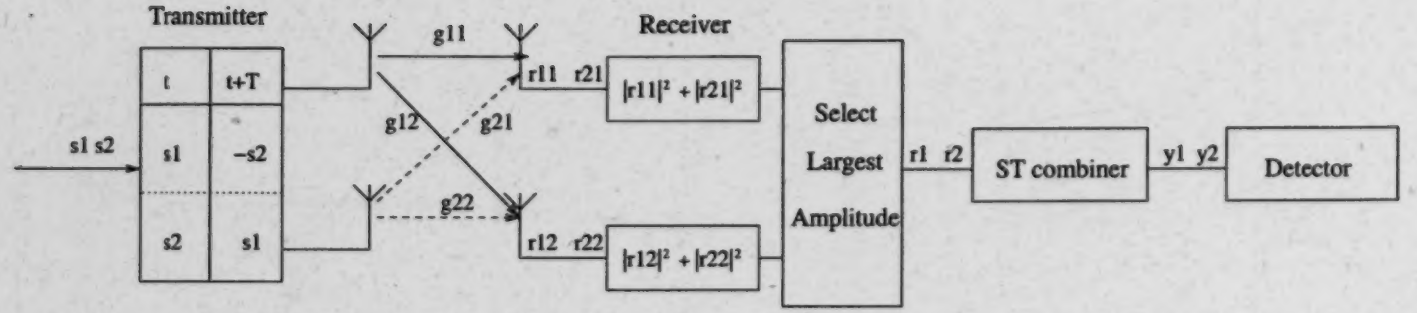

Fig. 5.1. The STSL receiver selection system model.

and, observe further that $s_1 + s_2 = \pm 2$ *and* $s_1 - s_2 = 0$, or $s_1 + s_2 = 0$ *and* $s_2 - s_1 = \pm 2$, so that

$$|r_{1,i} + r_{2,i}|^2 + |r_{1,i} - r_{2,i}|^2 = \tag{5.1b}$$
$$\begin{cases} \left|\pm 2g_{1,i} + n_{1,i} + n_{2,i}\right|^2 + \left|\pm 2g_{2,i} + n_{1,i} - n_{2,i}\right|^2, s_1 = -s_2 \\ \left|\pm 2g_{2,i} + n_{1,i} + n_{2,i}\right|^2 + \left|\pm 2g_{1,i} + n_{1,i} - n_{2,i}\right|^2, s_1 = s_2. \end{cases}$$

Thus, selecting the branch having the maximum value of $|r_{1,i}|^2 + |r_{2,i}|^2$ is equivalent to selecting the branch with the maximum value of

$$\left|g_{1,i} + n_1^e\right|^2 + \left|g_{2,i} + n_2^e\right|^2 \tag{5.2}$$

where n_1^e and n_2^e are independent, complex noise samples, each of variance $\frac{\sigma_n^2}{2}$ in each of the real and imaginary components. Observe that when the SNR becomes large, STSL selection becomes *SNR*-based selection because the noise terms in (5.2) become small. Observe further that the noise affecting the branch selection is effectively reduced by 3 dB in the STSL combiner.

The simulation results in the following section show that STSL selection has essentially the same performance as *SNR*-based selection.

5.2.2 Method 2: Space-Time Magnitude Selection

The proposed STSL selection combining scheme, which selects the branch providing the largest sum of $|r_{1,i}|^2 + |r_{2,i}|^2$, requires squaring the amplitudes of the received bit signals before making the selection. In order to further simplify the hardware implementation, we propose another scheme which selects the branch with the largest sum, $|r_{1,i}| + |r_{2,i}|$. Similar to STSL selection, this scheme, called space-time magnitude selection, does not require channel estimation. It is simpler than STSL selection because the receiver only needs to drop the sign of the two received signals $r_{1,i}$ and $r_{2,i}$, and then take the sum. The simulation results in the following section show that it has only slightly poorer BER performance than STSL and SNR selection. The system model is shown in Fig. 5.2.

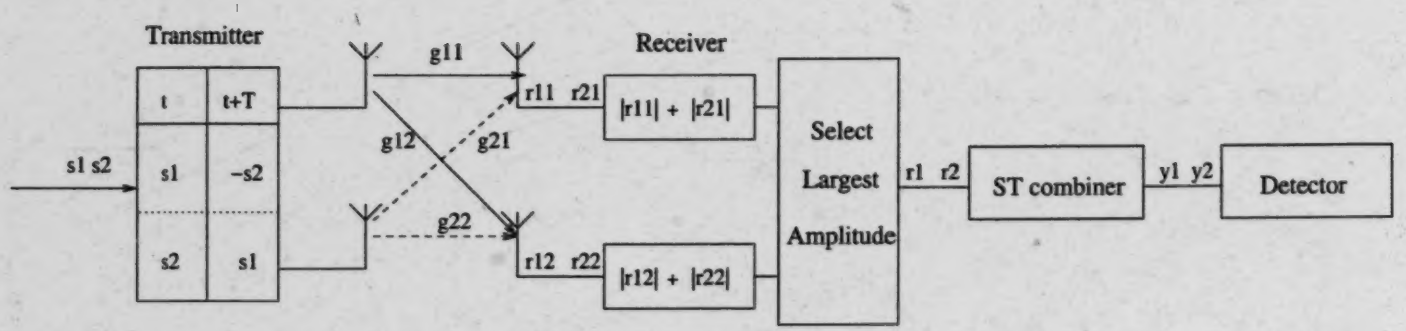

Fig. 5.2. The STM receiver selection system model.

5.3 Numerical results and discussion

In this section, all the figures are generated from Mento Carlo simulation by using Matlab. The number of simulation run times is equal to $\frac{10^3}{P_T}$, where P_T is the target error probability.

The BER results in this paper are functions of $\bar{\gamma}_c$, which is in turn a function of ρ and $\bar{\gamma}$. Fig. 5.3, Fig. 5.4 and Fig. 5.5 show plots of the average BER versus SNR per bit for the different selection diversity schemes in a flat Rayleigh fading channel with perfect channel estimation, cross-correlation 0.9, and cross-correlation 0.75, respectively. The *envelope*-selection, STSL selection and STM selection schemes are evaluated by computer simulation. As expected, these results show that, in all cases, the BER increases with increasing fading estimation error (decreasing value of ρ).

It is observed in Figs. 5.3-5.5, that the performances of LLR selection and MRC are the same for dual diversity. The performances are, indeed, identical because, for MRC the sign of the combiner output $Re(y_{1,1}) + Re(y_{1,2})$ is determined by the maximum of $Re(y_{1,i})$, which coincides with the LLR selection rule. It is also observed in Figs. 5.3- 5.5 that the performances of STSL selection and SNR selection are the same, at least to graphical accuracy. The STM selection scheme performs almost as well as the STSL and SNR selection schemes although it is simpler than both to implement. The biggest power penalty between STM and STSL is only less than 0.6 dB, which occurs with perfect channel estimation at 10 dB per bit. As does STSL selection, STM selection choses the best branch without requiring any channel estimation. The envelope-LLR selection scheme, which does require channel estimation of all the channels, performs better than the STSL, STM and SNR selection schemes but not as well as the LLR and MRC designs. The SSC selection scheme offers the poorest performance, in exchange for its simplicity, as expected.

Figs. 5.6, 5.7, and 5.8 show the average BER as a function of SNR per bit for the various selection schemes used in 4-fold diversity with perfect channel estimation, $\rho = 0.9$, and $\rho = 0.75$, respectively. There are a number of interesting observations. First, MRC and LLR are not the same, and MRC outperforms LLR, as expected. Second, the LLR selection outperforms envelope-LLR selection, as one expects. Third, the envelope-LLR selection

outperforms STSL, STM and SSC. Fourth, the performances of SNR and STSL selection are the same, as they were for the dual-branch case. This is a significant result. In order to implement SNR selection, the gains of all the diversity channels must be estimated. No channel estimation is required to implement STSL selection. The demodulation will require channel estimation according to (3.2), but in the case of STSL only two channel gains need to be estimated, while in the case of SNR selection, 2L channel gains must be estimated to implement the branch selection. Last, STM offers a less than 1.6 dB reduction of power compared to STSL, with a simpler implementation.

Figs. 5.3-5.8 show the average BER vs. SNR for specific, constant values of ρ. These results show clearly the performance differences between the selection schemes. They are also representative of a situation where the receiver electronics has reached a limit and cannot provide a better estimate of the channel gain. On the the other hand, many practical estimators will show a dependence on SNR, i.e. give better estimates as the SNR increases. In these cases, a larger SNR value leads to a better channel estimate, which means a higher value of ρ. To show this effect on BER, we consider PSAM as an example. We assume that a sinc interpolator with a Hamming window is used to interpolate fading estimates, with a frame size of 14, and normalized Doppler shift of 0.03. Fig. 5.9 shows the average BER versus SNR from 0 dB to 10 dB with $L = 2$. Since ρ is also a function of the symbol location, that is, with the same SNR value, in the same frame, data symbols located at different places will experience different ρ values; we give the BER of the 3rd data symbol in a frame as an example. Computed from (3.14), the value of ρ for this PSAM system varies from 0.513 to 0.913 as the SNR varies from 0 dB to 10 dB. Similar to the results in Figs. 5.3-5.5, in Fig. 5.9, MRC and LLR selection still have the best performance, then envelope-LLR selection outperforms SNR and STSL selection, which in turn slightly outperform STM selection. The simplest selection scheme, SSC selection, has the worst BER performance. Again, the performance of SNR and STSL schemes are indistinguishable. Fig. 5.10 shows similar results for 4-fold diversity. In this case, MRC outperforms LLR selection, but SNR and STSL selection again have the same performance, which is marginally better than STM selection.

5.4 Conclusion

A new selection scheme, STSL selection, was proposed with a much simpler hardware implementation for Alamouti transmission systems. The results show that it has the same performance as SNR selection. A suboptimal selection scheme, STM, was also proposed with a still simpler implementation, but only slightly poorer performance than STSL selection combining. The BER results of these two new schemes were compared quantitatively with those of LLR selection, SNR selection, SSC selection and MRC.

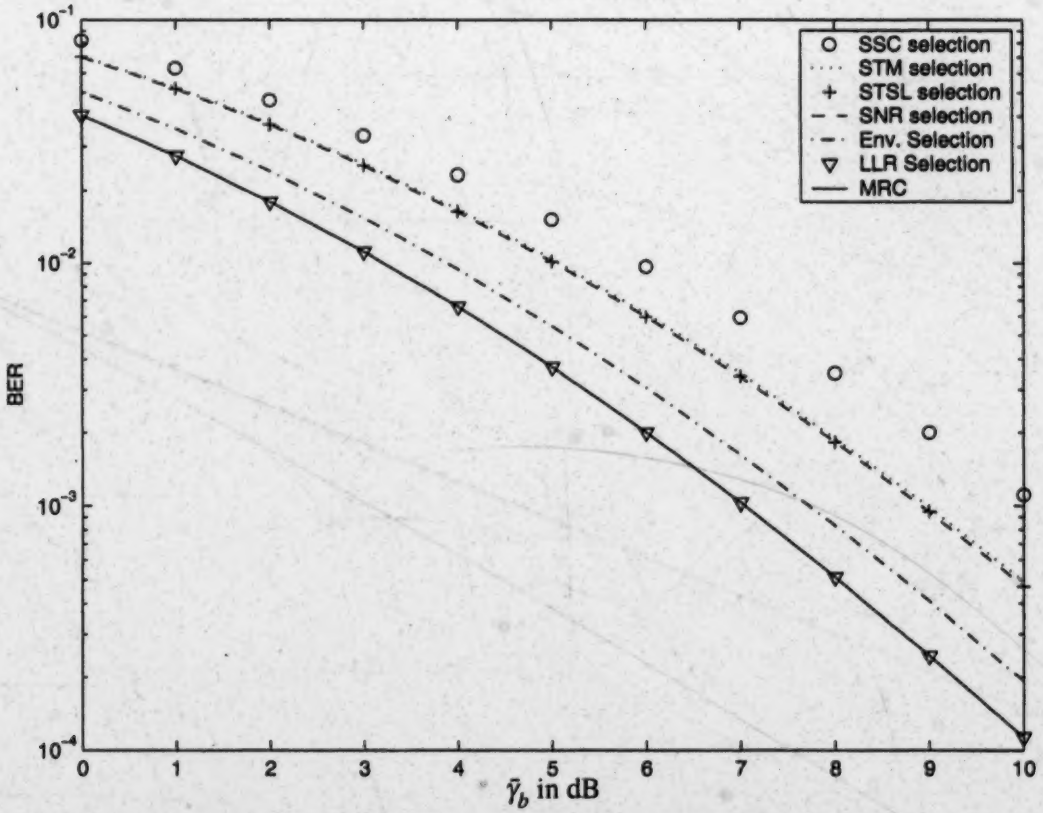

Fig. 5.3. The BER versus SNR for the 2 TX and 2 Rx, space-time block code with perfect channel estimation.

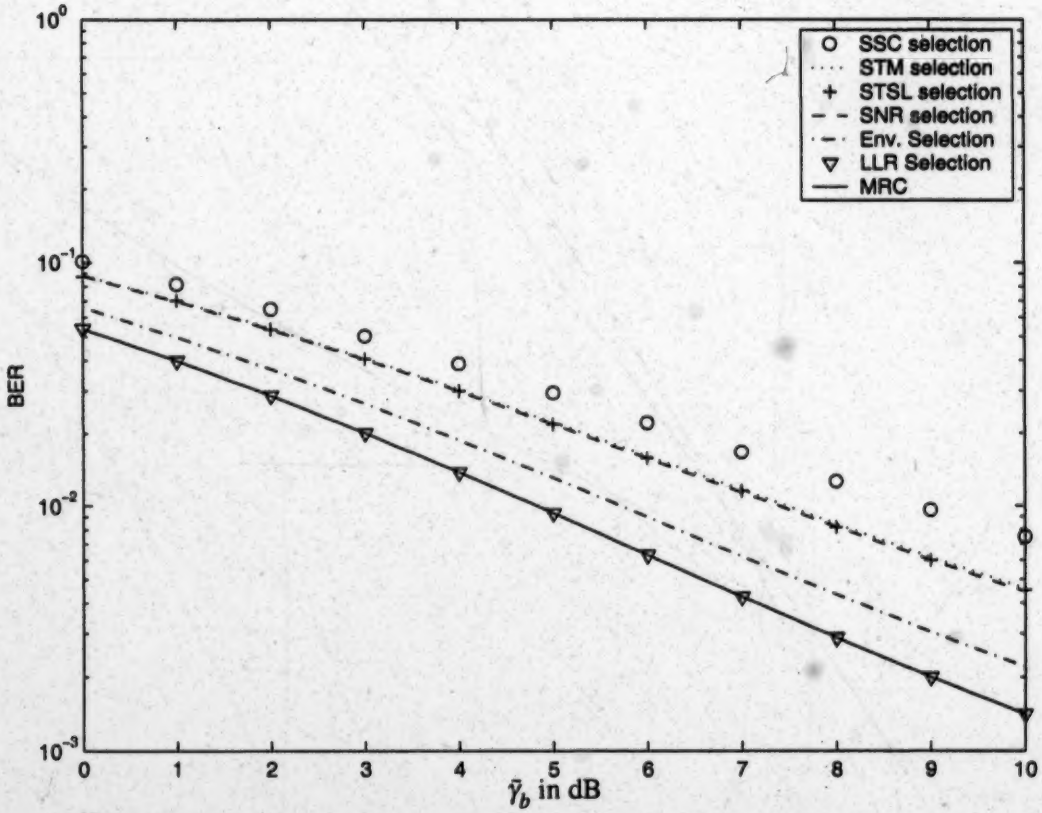

Fig. 5.4. The BER versus SNR for the 2 TX and 2 Rx, space-time block code with ρ=0.9.

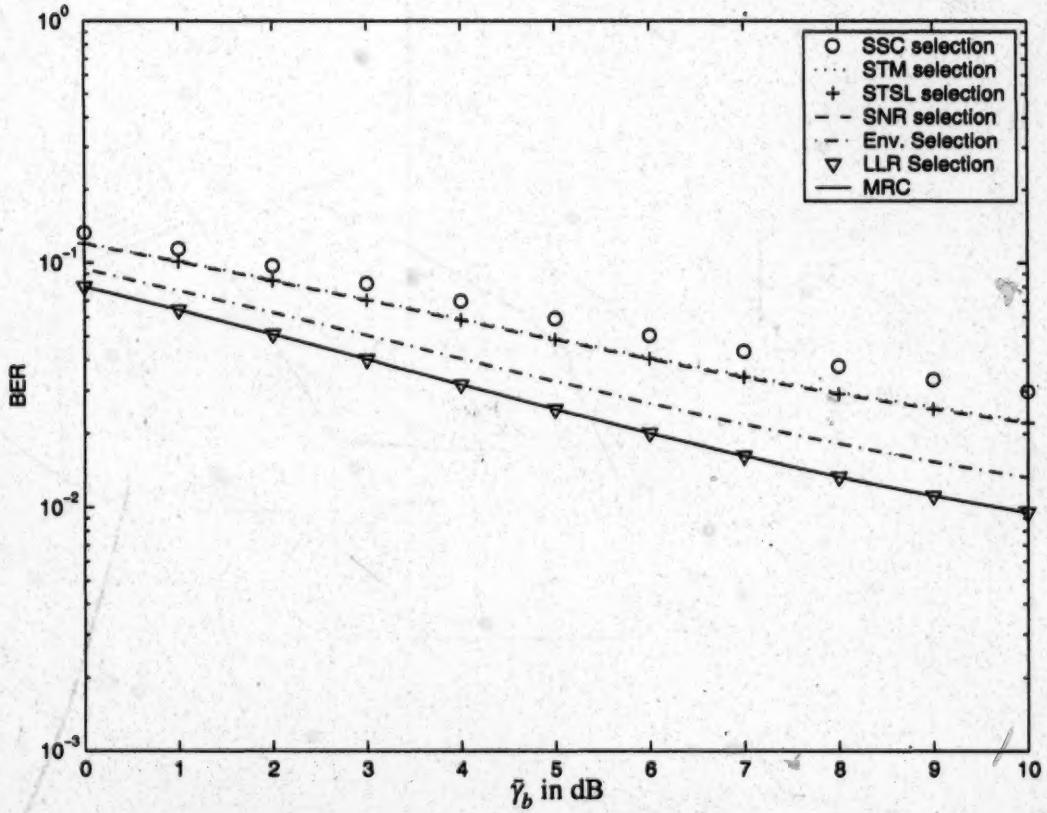

Fig. 5.5. The BER versus SNR for the 2 TX and 2 Rx, space-time block code with ρ=0.75.

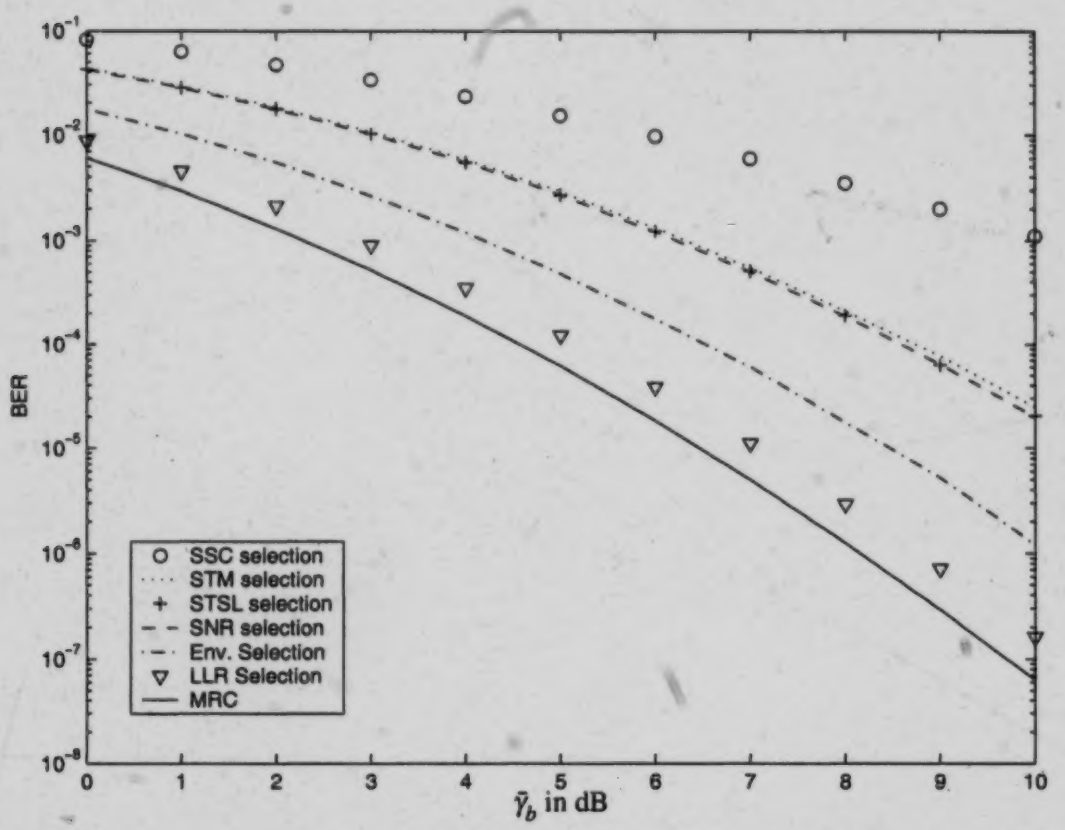

Fig. 5.6. The BER versus SNR for the 2 TX and 4 Rx, space-time block code with perfect channel estimation.

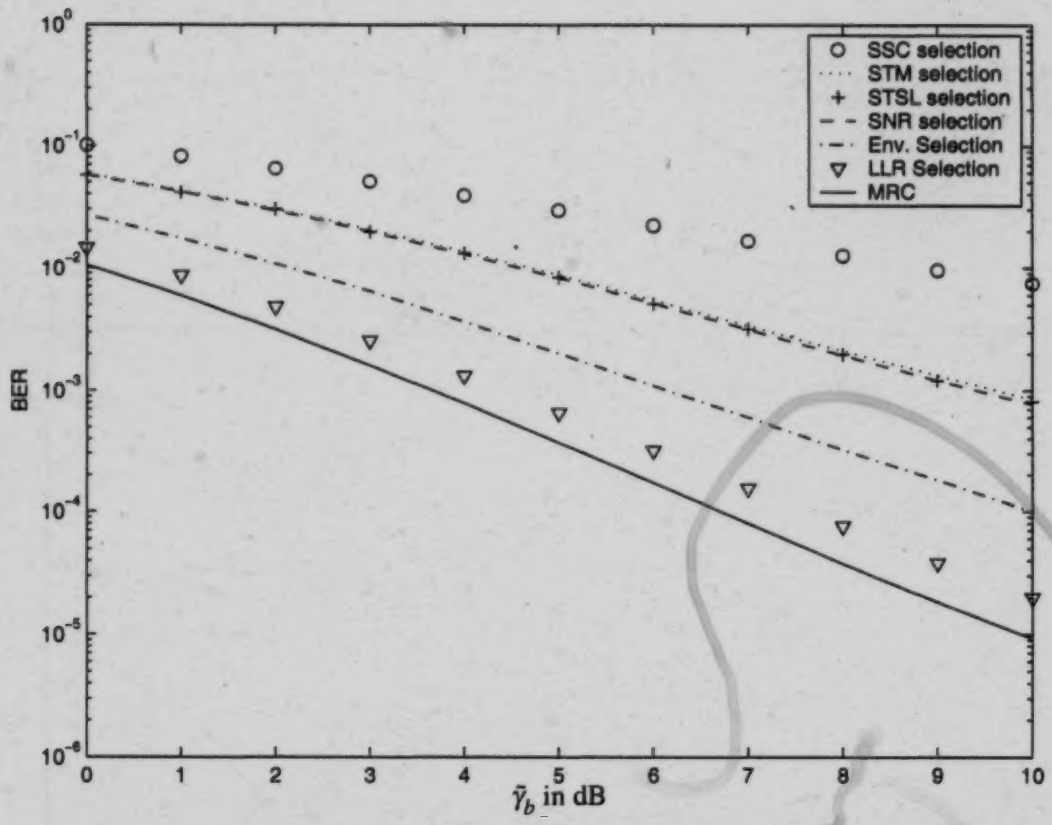

Fig. 5.7. The BER versus SNR for the 2 TX and 4 Rx, space-time block code with ρ=0.9.

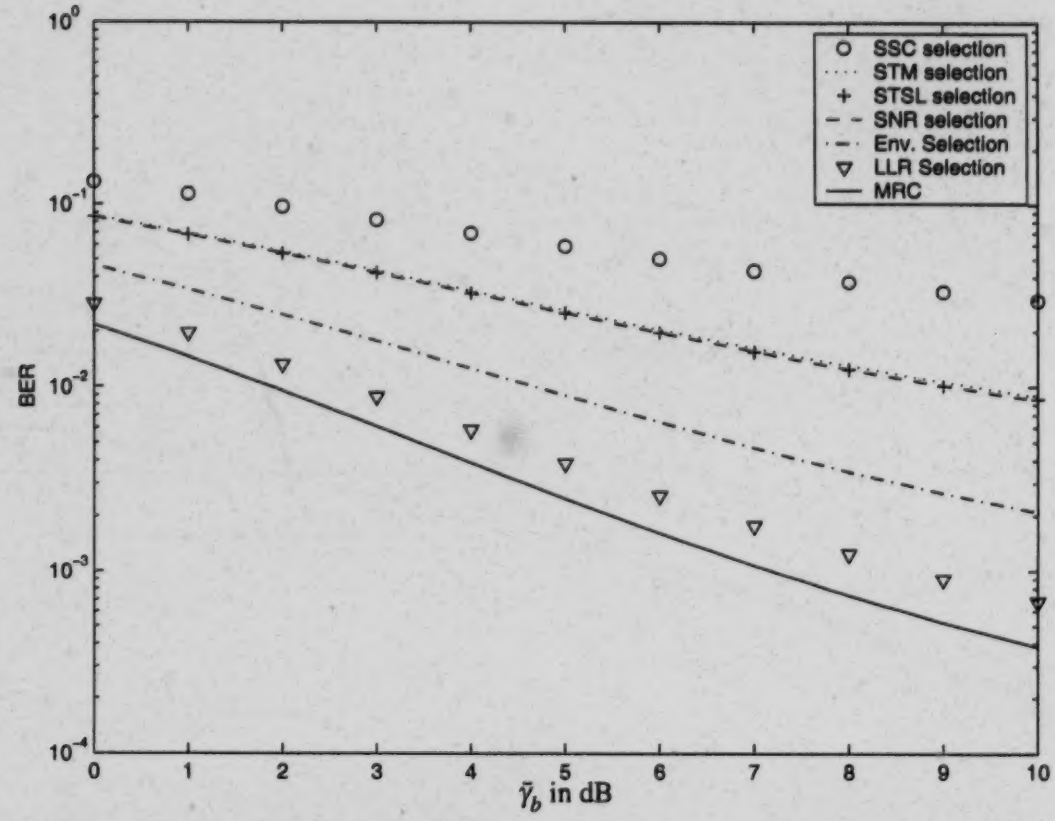

Fig. 5.8. The BER versus SNR for the 2 TX and 4 Rx, space-time block code with ρ=0.75.

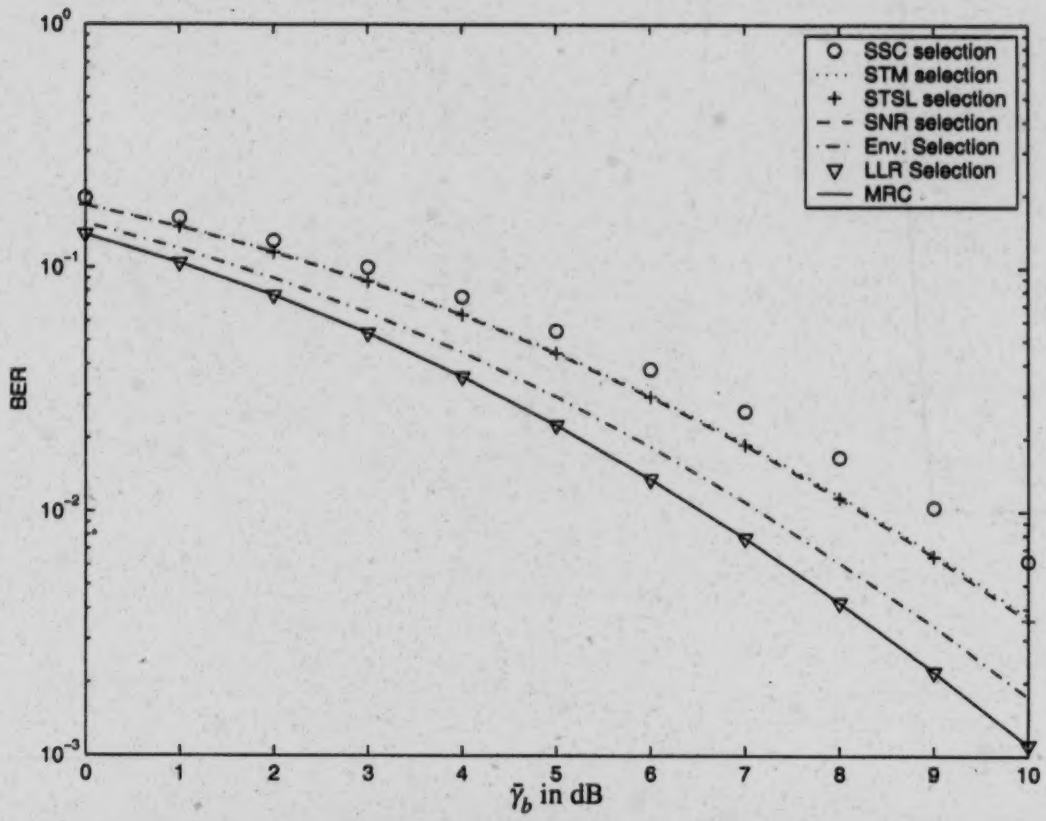

Fig. 5.9. The PSAM BER versus SNR for the 2 TX and 2 Rx, space-time block code with Hamming windowing applied to a sinc interpolator for $K = 30$, $N = 14$ and $f_D T_s = 0.03$ with symbol location at $n = 3$.

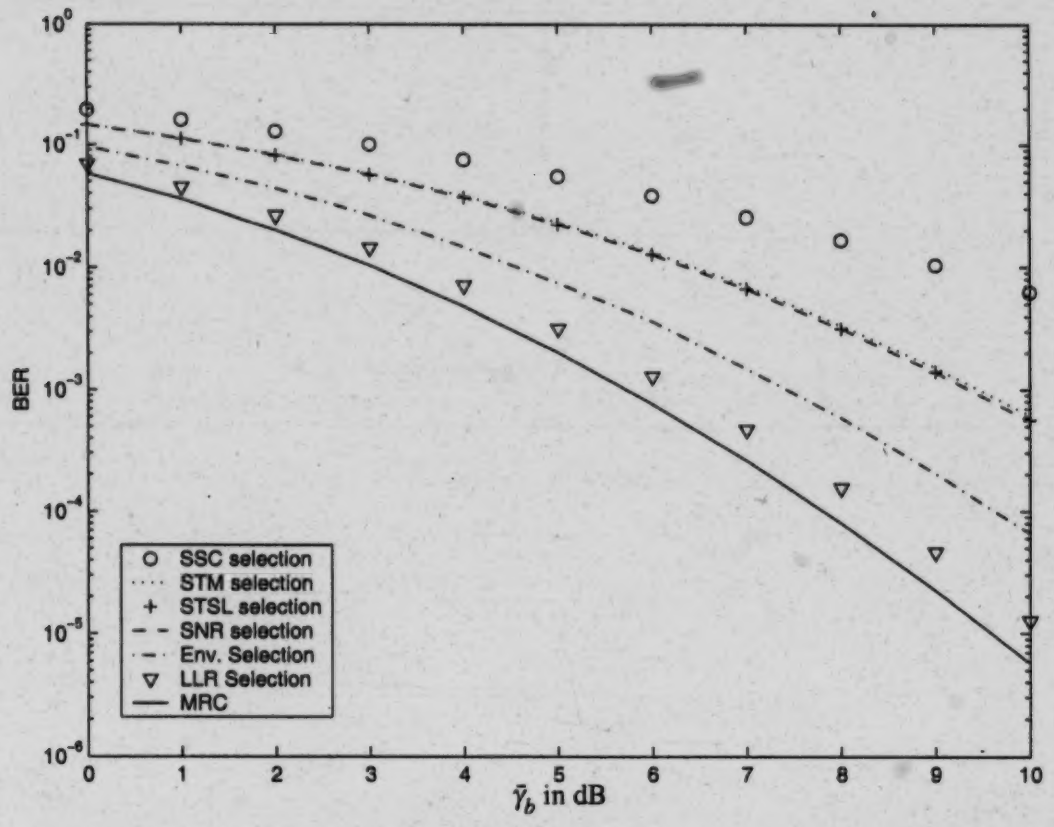

Fig. 5.10. The PSAM BER versus SNR for the 2 TX and 4 Rx, space-time block code with Hamming windowing applied to a sinc interpolator for $K = 30$, $N = 14$ and $f_D T_s = 0.03$ with symbol location at $n = 3$.

Chapter 6

Conclusions

Multiple antenna diversity methods can improve wireless system performance. It exploits the multiple paths between transmitters and receivers through space-time coding techniques to reduce the BER. However, the implementation of multiple antennas requires multiple RF chains (consisting of amplifiers, analog-to-digital converters, etc.) that are typically very expensive. This, therefore, stimulates the need for low-cost, low-complexity techniques with the benefits of multiple antennas. Antenna selection is one such technique because an antenna selection element is typically much cheaper than RF chains and its system performance is only slightly poorer than that of the full-complexity system. With antenna selection, transmission/reception is performed through the optimal antenna subset.

Early work in antenna selection has concentrated on the MISO channel or the SIMO channel. In our research, the selection is implemented at the receiver side in a MIMO system using the Alamouti scheme. This is relatively new and only few papers have investigated this area.

The traditional selection scheme selects antenna branches with the largest SNR. However, this method is not, all the time, the simplest and/or the one which offers the best performance. There are several other selection schemes that have been proposed by different authors: e.g. LLR selection, $S+N$ selection, etc. In this thesis, these selection schemes were re-examined and compared using Alamouti transmission scheme. In addition to the

existing selection schemes, two new selection schemes for Alamouti MIMO system were proposed and analyzed.

In practice, the complex channel gains have to be estimated at the receiver to be able to implement the selection algorithm. As a result of noisy channel estimates, system performance degrades compared to that of system with perfect channel estimation. Thus, the effect of channel estimation error on this Alamouti MIMO system was investigated. The estimation error using PSAM on Alamouti MIMO systems using different selection methods was illustrated. In summary:

1. Channel estimation using PSAM in flat Rayleigh fading with the Alamouti system was investigated. The PSAM signal frame structure was defined assuming slow Rayleigh fading and the Alamouti transmission scheme. The squared cross-correlation coefficient of the channel fading and its estimate, ρ, for PSAM in Alamouti system was derived. The value of ρ ranges from 0 to 1, representing the poorest estimation to perfect channel estimation, respectively. This expression was used to quantify the estimation error for LLR selection, envelope-LLR selection, SNR selection, SSC selection, STSL selection, STM selection, and MRC.

2. The BER of BPSK in Rayleigh fading using the Alamouti transmission scheme and receiver selection diversity in the presence of channel estimation error was studied. Various selection schemes: LLR selection, Env-LLR selection, SNR selection, SSC and MRC were considered in this scheme. The exact, closed-form expressions for the BER of LLR selection, SNR selection, SSC selection and MRC were derived in terms of the SNR along with the cross-correlation coefficient of the channel gain and its corrupted estimate. The BER of Env-LLR selection was simulated.

3. Two new receiver selection schemes, STSL selection diversity and STM selection diversity, were proposed for a MIMO system using the Alamouti space-time block code at the transmitter in a slow, flat Rayleigh fading channel. They were proved to provide almost the same performance as SNR selection, but with much simpler

implementations. The BER of BPSK in Rayleigh fading using these two selection schemes was simulated.

4. All presently existing selection schemes and the two new schemes were compared with both perfect and imperfect channel estimation. First, the effects of channel estimation errors on each selection scheme were examined with constant values of ρ. This allowed a comparison between all selection systems when they offer the same ρs. Then, considering a PSAM estimator with a sinc interpolator and a Hamming window, the BER performances were compared under different Doppler shifts and frame sizes.

References

[1] S. M. Alamouti, "A simple transmit diversity technique for wireless communications," *IEEE J. Select. Areas Commun.*, vol. 16, no. 8, pp. 1451–1458, Oct. 1998.

[2] J. G. Proakis, *Digital Communications*. McGraw-Hill, 1995.

[3] A. F. Molisch and M. Z. Win, "MIMO systems with antenna selection–and overview," Mitsubishi electric research labs, Tech. Rep., Mar. 2004.

[4] S. Sanayei and A. Nosratinia, "Antenna selection in MIMO systems," *IEEE Communications Magazine*, pp. 68–73, Oct. 2004.

[5] A. F. Molisch, M. Z. Win, and J. H. Winters, "Capacity of MIMO systems with antenna selection," in *Proc. IEEE Int. Conf. on Commun. ICC 2001*, vol. 2, June 2001, pp. 570–574.

[6] A. Gorokhov, D. Gore, and A. Paulraj, "Receiver antenna selection for MIMO flat-fading channels: theory and algorithms," *IEEE Trans. Inform. Theory*, vol. 49, no. 10, pp. 2687–2696, Oct. 2003.

[7] M. Gharavi-Alkhansari and A. B. Gershman, "Fast antenna subset selection in MIMO systems," *IEEE Trans. Sig. Proc.*, vol. 52, no. 2, pp. 339–347, Feb. 2004.

[8] A. Ghrayeb and T. M. Duman, "Performance analysis of MIMO systems with antenna selection over quasi-static fading channels," *IEEE Trans. Veh. Technol.*, vol. 52, no. 2, pp. 281–288, Mar. 2003.

[9] I. Bahceci, T. M. Duman, and Y. Altunbasak, "Antenna selection for multiple-antenna transmission systems: performance analysis and code construction," *IEEE Trans. Inform. Theory*, vol. 49, no. 10, pp. 2669–2681, Oct. 2003.

[10] X. Zeng and A. Ghrayeb, "Performance bounds for space-time block codes with receive antenna selection," *IEEE Trans. Inform. Theory*, vol. 50, no. 9, pp. 2130–2137, Sep. 2004.

[11] D. A. Gore, R. U. Nabar, and A. Paulraj, "Selecting an optimal set of transmit antennas for a low rank matrix channel," in *Proc. IEEE Int. Conf. on Acoustics, Speech, and Signal Processing ICASSP 2000*, vol. 5, June 2000, pp. 2785 –2788.

[12] S. Sandhu, R. U. Nabar, D. A. Gore, and A. Paulraj, "Near-optimal selection of transmit antennas for a MIMO channel based on shannon capacity," in *Proc. 34th Asilomar Conf. on Signals, Systems and Computers*, vol. 1, 29 Oct.-1 Nov. 2000, pp. 567–571.

[13] D. A. Gore, R. W. Heath, and A. J. Paulraj, "Transmit selection in spatial multiplexing systems," *IEEE Communications Letters*, vol. 6, no. 11, pp. 491–493, Nov. 2002.

[14] D. Gore and A. Paulraj, "Space-time block coding with optimal antenna selection," in *Proc. IEEE Int. Conf. on Acoustics, Speech, and Signal Processing*, vol. 4, May 2001, pp. 2441–2444.

[15] A. Thoen, L. V. der Perre, B. Gyselinckx, and M. Engels, "Performance analysis of combined transmit-sc/receive-mrc," *IEEE Trans. Commun.*, vol. 49, no. 1, pp. 5–8, Jan. 2001.

[16] A. Molisch, M. Win, and J. Winters, "Reduced-complexity transmit/receive-diversity systems," *IEEE Trans. Sig. Proc.*, vol. 51, no. 11, pp. 2729–2738, Nov. 2003.

[17] Z. Chen, "Asymptotic performance of transmit antenna selection with maximal-ratio combining for generalized selection criterion," *IEEE Communications Letters*, vol. 8, no. 4, pp. 247–249, Apr. 2004.

[18] D. Gore and A. Paulraj, "Statistical MIMO antenna sub-set selection with space-time coding," in *Proc. IEEE Int. Conf. on Communications ICC 2002*, vol. 1, 28 Apr.-2 May 2002, pp. 641–645.

[19] D. Gore, R. Heath, and A. Paulraj, "Statistical antenna selection for spatial multiplexing systems," in *Proc. IEEE Int. Conf. on Commun. ICC 2002*, vol. 1, 28 Apr.-2 May 2002, pp. 641–645.

[20] D. A. Gore and A. J. Paulraj, "MIMO antenna subset selection with space-time coding," *IEEE Trans. Sig. Proc.*, vol. 50, no. 10, pp. 2580–2588, Oct. 2002.

[21] R. S. Blum and J. H. Winters, "On optimum MIMO with antenna selection," *IEEE Communications Letters*, vol. 6, no. 8, pp. 322–324, Aug. 2003.

[22] J. D. Gibson, Ed., *The mobile communications handbook*, 2nd ed. Boca Raton, FL: CRC Press, 1999.

[23] T. S. Rappaport, *Wireless communications Principles and Practice*, 2nd ed. Prentice Hall, 2002.

[24] W. C. Jakes, *Microwave Mobile Communications*. Piscataway, NJ: IEEE Press, 1993.

[25] W. Lee, *Mobile Communications Engineering*. New York: McGraw-Hill, 1982.

[26] M.-S. Alouini and M. K. Simon, "An MGF-based performance analysis of generalized selection combining over Rayleigh fading channels," *IEEE Trans. Commun.*, vol. 48, no. 3, pp. 401–415, Mar. 2000.

[27] J. N. Pierce, "Theoretical diversity improvement in frequency-shift keying," in *Proc. IRE*, vol. 46, May 1958, pp. 903–910.

[28] E. A. Neasmith and N. C. Beaulieu, "New results on selection diversity," *IEEE Trans. Commun.*, vol. 46, no. 5, pp. 695–703, May 1998.

[29] T. Eng, N. Tong, and L. B. Milstein, "Comparison of diversity combining techniques for Rayleigh-fading channels," *IEEE Trans. Commun.*, vol. 44, pp. 1117–1129, Sep. 1996.

[30] S. W. Kim and E. Y. Kim, "Optimum selection diversity for BPSK signals in Rayleigh fading channels," *IEEE Trans. Commun.*, vol. 49, no. 10, pp. 1715–1718, Oct. 2001.

[31] G. Foschini and M. Gans, "On the limits of wireless communications in a fading environment when using multiple antennas," *Wireless Personal Commun.*, vol. 6, no. 3, pp. 311–335, Mar. 1998.

[32] V. Tarokh, H. Jafarkhani, and A. R. Calderbank, "Space-time block code from orthogonal designs," *IEEE Trans. Inform. Theory*, vol. 45, pp. 1456–1467, July 1999.

[33] M. J. Gans, "The effect of Gaussian error in maximal ratio combiners," *IEEE Trans. Commun. Technol.*, vol. 19, no. 4, pp. 492–500, Aug. 1971.

[34] G. L. Stüber, *Principles of Mobile Communication*, 2nd ed. MA:Kluwer: Norwell, 2001.

[35] L. Cao and N. C. Beaulieu, "Exact error-rate analysis of diversity 16-QAM with channel estimation error," *IEEE Trans. Commun.*, vol. 52, no. 6, pp. 1019–1029, June 2004.

[36] J. K. Cavers, "An analysis of pilot symbol assisted modulation for Rayleigh fading channels," *IEEE Trans. Veh. Technol.*, vol. 40, no. 11, pp. 686–693, 1991.

[37] Y.-S. Kim, C.-J. Kim, G.-Y. Jeong, Y.-J. Bang, H.-K. Park, and S. S. Choi, "New Rayleigh fading channel estimator based on PSAM channel sounding technique," in *Proc. IEEE Int. Conf. on Communications ICC 1997*, vol. 3, June 1997, pp. 1518–1520.

[38] S. W. Kim and E. Y. Kim, "Optimum receive antenna selection minimizing error probability," in *Proc. Wireless Communications and Networking Conference*, vol. 1, Mar. 2003, pp. 441–447.

[39] M. A. Blanco and K. J. Zdunek, "Performance and optimization of switched diversity systems for the detection of signals with Rayleigh fading," *IEEE Trans. Commun.*, vol. 27, pp. 1887–1895, Dec. 1979.

[40] A. A. Abu-Dayya and N. C. Beaulieu, "Analysis of switched diversity systems on generalized-fading channels," *IEEE Trans. Commun.*, vol. 42, no. 11, pp. 2959–2966, Nov. 1994.

[41] I. S. Gradshteyn and I. M. Ryzhik, *Table of Integral, Series, and Products*, 6th ed., A. Jeffrey and D. Zwillinger, Eds. Academic Press, 2000.

[42] H. A. David, *Order Statistics*. New York: Wiley, 1981.